Characterization of Structurally-Enhanced Solder Joints Using Vertically-Aligned Carbon Nanotubes

by

Melissa Amy Peacock

A thesis submitted to the Graduate Faculty of
Auburn University
in partial fulfillment of the
requirements for the Degree of
Master of Science

Auburn, Alabama
August 2, 2014

Keywords: thermal interface materials, carbon nanotubes, electronics cooling

Approved by

Daniel K. Harris, Chair, Associate Professor of Mechanical Engineering
Robert L. Jackson, Associate Professor of Mechanical Engineering
Virginia Davis, Professor of Chemical Engineering

Abstract

Since the demand for more efficient means of electronics cooling has grown significantly over recent years, the need for more advanced thermal interface materials has also increased. Thermal interface materials (TIMs) are a vital part of electronics cooling. TIMs are materials that are used to fill in the microscopic spaces that exist between electronic circuits and heat sink surfaces due to surface roughness or other surface imperfections. Additionally, TIMs are used to promote effective thermal transport across interfaces. In general, materials that have high thermal conductivities and low thermal resistances are ideal for use as TIMs. The thermal performance of a TIM is typically characterized by its thermal conductivity and thermal resistance, which are both measurements of how well heat travels through a medium.

Carbon nanotubes (CNTs) have been reported to possess very good thermal and mechanical properties. For example, the theoretical thermal conductivity of an individual single-walled CNT has been calculated to be 37,000 $\frac{W}{m-K}$ [1]. Experimental thermal conductivity values have been found in the range of 25 $\frac{W}{m-K}$ to 267 $\frac{W}{m-K}$. These values are influenced by parameters such as the alignment and quality of CNTs. Furthermore, CNTs have been found to have good compliancy and resiliency, which are also ideal traits for TIM applications. Not only do these characteristics make CNTs excellent candidates for TIMs, but they also make them promising for use in solder joint enhancement. This is due to the fact that a common drawback concerning solder joints in electronics packaging is coefficient of thermal expansion (CTE) mismatches, which frequently result in solder joint failure. Incorporating CNTs into a solder interface could potentially extend the life of the solder joint by making it stronger and more pliable.

In this study, a solder-CNT composite TIM was fabricated using vertically-aligned carbon nanotubes (VACNTs) due to the intrinsically high thermal conductivity of carbon nanotubes (CNTs). The constructed TIM consisted of vertically-aligned carbon nanotube arrays (VACNAs), which were grown by chemical vapor deposition (CVD), soldered to copper disks on both sides via a bismuth/tin/silver solder. Soldering the free ends of the CNTs overcame one of the major contributors to thermal resistance, which is the contact resistance between the CNT free ends and an opposing substrate. The thermal performance potential of the produced sample as a TIM was measured using an Analysis Tech ASTM 5470 Thermal Interface Material Tester. This apparatus measured the thermal resistance and thermal conductivity of the constructed TIM, and it also analyzed the pressure dependence of the thermal properties. The interfacial thermal resistance of the CNT-solder composite was examined and reported for pressures of 20 psi and 50 psi. The average thermal resistance value recorded for the constructed sample was 0.458 $\frac{cm^2-K}{W}$ at a pressure of 20 psi and 0.435 $\frac{cm^2-K}{W}$ at a pressure of 50 psi.

Acknowledgments

The completion of this Master's thesis symbolizes much more than simply the last step in obtaining a Master's degree in Mechanical Engineering. Because I was a non-traditional student coming from a Mathematics background, I had a lot to learn before I could officially enter Auburn's Mechanical Engineering graduate program. Firstly, I thank my adviser Dr. Daniel K. Harris for providing me with the opportunity to pursue this degree. I also thank Dr. Harris for believing in my ability to complete this degree and for investing his time to help me to accomplish my goals.

I would also like to thank Dr. Virginia Davis for her contributions to my research involving carbon nanotubes. Her expertise has been a great asset to my research. I thank both Dr. Virginia Davis and Dr. Robert Jackson for serving on my committee for my thesis defense.

Additionally, I thank the professors Charles Ellis, Michael Hamilton, Mike Palmer, and Hulya Kirkici, along with their involved students, in the Electrical Engineering department for their contributions to my research. I also thank Suzie Murdock for her contributions in my early research and Chandan Roy for assisting me with the thermal performance testing.

I thank my friends and family for their moral support. In particular, I thank Mr. Cecil Creel and Mrs. Alyson Creel for their unwavering support throughout my high school and college years. Their faith in me has truly helped me achieve my goals. I thank the friends that I have met in Auburn, especially the ones that allowed me to talk about carbon nanotubes and thermal interface materials with them. Furthermore, I thank my stepfather and mother for supporting me in any way that they could while I furthered my university studies.

Last but not least, I must give great thanks to my mom again for everything she has done for me. If it were not for her, I would not have been able to succeed in acquiring this

Master's degree. It was from her that I learned how to persevere through any and every hardship brought upon me. She has supported me unconditionally and made me the person I am today.

Table of Contents

List of Figures

List of Tables

Chapter 1

Introduction

When two solid objects are in mechanical contact with one another, and heat is being transferred across the common interface where the materials touch, a significant temperature drop at the interface between materials may exist. This is due to what is termed the thermal contact resistance between the surfaces of the separate materials. Thermal contact resistance is due to the surface roughness of materials as well as other mechanical misalignments. Because of surface roughness effects, there exist microscopic gaps at the material interfaces. These gaps are typically filled with air, which usually does not have a high enough thermal conductivity to meet heat removal requirements. Thermal interface materials (TIMs) are used to fill the air gaps with a more thermally conductive material and to create more contact points at the interface between materials, thereby decreasing the interstitial thermal resistance [4].

Some material properties desired for TIM applications are high thermal conductivities and high mechanical conformities in order to fill in interfacial gaps. Many conventional TIMs are a combination of metal particles with a base material, such as silicone oil. The metal particles provide high thermal conductivities while base materials offer high compliances. The best commercially available pastes and greases have thermal conductivities from 1 to 10 $\frac{W}{m-K}$ [5]. More recently, much research involving the use of carbon nanotubes (CNTs) as TIMs has been conducted.

While many helped pave the way to the discovery of the astonishing molecular structure known as the carbon nanotube, who should be credited with actually inventing the CNT is still controversial. Even though Sumio Iijima of IBM was credited with the development of the nanotube in 1991, Roger Bacon may have been the first scientist to produce CNTs in

the 1950s. Unfortunately for Bacon, he lacked the advanced electron microscope needed to assess his fabrication [6].

CNTs are tube-like structures composed of carbon atoms that can be described as a hexagonal net [7]. Single-walled carbon nanotubes (SWNTs) consist of a single-tube structure, while multi-walled carbon nanotubes (MWNTs) are comprised of concentric tube structures. The diameter of CNTs normally ranges from less than a nanometer to 50 nm, and their lengths can range from microns to centimeters.

Carbon nanotubes have been considered for applications in thermal management due to their intrinsically high thermal conductivity. According to Hone, theoretical calculations for an isolated SWNT suggest a thermal conductivity value of 37,000 $\frac{W}{m-K}$. This value is comparable to that of a diamond, for which the highest thermal conductivity value was measured to be 41,000 $\frac{W}{m-K}$. In one study, the measured thermal conductivity of a bulk sample of aligned SWNTs was found to be above 200 $\frac{W}{m-K}$ [8]. While investigating the thermal conductivity of individual MWNTs, Kim et al. reported a room-temperature thermal conductivity of 3000 $\frac{W}{m-K}$ [1].

CNTs also display remarkable mechanical properties. Not only do they have the potential to be stronger than steel, but they have also been observed to be extremely resilient. To perform well as a TIM, it is important that a material possess sufficient conformability to fill the microscopic spaces present at an interface. The fact that CNTs maintain required qualities for TIM use is supported by both theoretical models and experimental data. CNTs are able to adapt and conform to considerable external loads and still reestablish their initial form with no permanent atomic alterations [9].

In addition to their thermal and mechanical properties, it is practical to consider the electrical properties of CNTs when employing them in electronics packaging applications. CNTs have been studied for use in micro-electronics and nano-electronics due to their high electrical conductivities [10], which have been measured to be approximately 10^6-10^7 Siemens per meter (S/m) [11]. Their electrical conductivities are dependent on properties such as

nanotube diameter and chirality. Chirality describes the degree of twist in the CNT structure. For a temperature of 27°C, the electrical resistivity of SWNTs has been reported to be around 10^{-4} Ohm-cm, making SWNT ropes the most conductive carbon fibers identified [12].

Because of their excellent thermal properties, vertically-aligned carbon nanotube (VACNT) arrays show great potential for TIM applications. Ideally, carbon nanotube arrays (CNAs) would act as pathways for thermal transport. Factors that should be considered in the fabrication of CNAs include the alignment, quality, and density of the CNTs. These properties can be influenced by fabrication conditions. CNT entanglement results in a higher thermal resistance, and low quality CNTs would possess less than optimal thermal conductivities. A high density CNA is ideal so that more pathways for heat transport exist.

Another common material used for TIM applications is solder. Solder joints are often used in heat sink attachment interfaces and other electronic packaging interfaces [13]. An important aspect of electronic packaging is choosing materials that have compatible coefficients of thermal expansion [14]. The coefficient of thermal expansion (CTE) describes to what degree a material expands upon heating [15]. In surface-mount devices (SMDs), a solder joint is the mechanical connection as well as the electrical connection [14]. Thermal expansion mismatches in solder joints can lead to both deformation and failure, especially when subjected to temperature cycling. In particular, when a material with a significantly higher CTE is bonded to another material with a lower CTE, the material with a higher CTE is constrained during heating. This can result in deformation or cracking of the heat sink or device as well as failure of the solder joint [13]. Since CNTs possess good conformability as well as a high thermal conductivity, they could overcome the issue of CTE mismatches in solder joints by increasing the mobility of the joint and prolonging the life of the joint before failure without hindering heat transfer across the interface.

Chapter 2

Literature Review

The demand for more efficient means for cooling electronics has increased significantly over recent years. Thermal interface materials (TIMs) are an important area of study in thermal management. Since power densities have been predicted to grow substantially in upcoming years, more advanced techniques for thermal management are being explored. These materials are used to fill in the microscopic spaces that exist between electronic circuits and heat sink surfaces due to surface roughness and to promote efficient thermal transport. Generally, materials that have high thermal conductivities are ideal for use as TIMs. Thermal conductivity and thermal resistance are both measurements of how well heat travels through a medium. Some commercial TIMs include thermal greases, thermal putties, and phase change materials (PCMs) in which the thermal conductivities usually range from 1 to 10 $\frac{W}{m-K}$ [5]. Due to their excellent thermal and mechanical properties, carbon nanotubes (CNTs) are potential candidates for novel and highly effective TIMs.

When considering using CNTs as TIMs, aligned CNTs are ideal in order to promote better thermal transport. When the thermal conductivity of bulk samples of single-walled carbon nanotubes (SWNTs) was experimentally tested, a thermal conductivity of about 35 $\frac{W}{m-K}$ was observed. The low thermal conductivity value was attributed to the fact that the SWNTs were highly tangled in this sample. After aligning the nanotubes, the thermal conductivity was increased to a thermal conductivity value over 200 $\frac{W}{m-K}$ [1]. Therefore, vertically-aligned CNTs (VACNTs) are superior to randomly-aligned CNTs for TIM applications because heat can travel through VACNTs much more efficiently.

The thermal conductivity of multi-walled carbon nanotubes (MWNTs) was also found experimentally by Yi et al. For bulk samples of MWNTs, a thermal conductivity value of

around 25 $\frac{W}{m-K}$ was determined. This low value may have been due to the contact between nanotubes. For individual MWNTs, Kim et al. obtained a thermal conductivity value over 3000 $\frac{W}{m-K}$ [1].

Very high thermal conductivity values have been reported for individual CNTs. However, measured thermal conductivity values for bundled CNTs are much lower due to factors such as tube-tube resistances and radiation heat losses. Aliev et al. [16] reported a thermal conductivity of approximately 600 $\frac{W}{m-K}$ for individual MWNTs and 150 $\frac{W}{m-K}$ for MWNT bundles. Tube-tube interconnections and CNT structural defects decreased thermal conductivity values to 50 $\frac{W}{m-K}$ for MWNT sheets. According to Aliev et al. [16], MWNTs are superior to SWNTs for thermal transport purposes since MWNTs offer more paths for phonons to detour the characteristic defects of the nanotubes [16].

Zhang et al. [17] conducted an experiment to investigate the thermal conductivity of MWNT films using a pulsed photothermal reflectance (PPR) method, where heat conduction was assumed to be one dimensional and heat losses were neglected. The tested configuration, an Au/CNT/Si structure, employed high resistivity silicon substrates with indentations that were chemically etched into them. Nickel films, varying from 0.5 to 100 nm, were deposited into the indentations of the substrate and used as catalysts for CNT growth. CNTs were synthesized by microwave plasma chemical vapor deposition at 720°C for 10 minutes. The lengths of the fabricated MWNTs ranged from 10-50 μm, and their diameters ranged from 40-100 nm. The final step in the process was affixing a 1.2 μm thick gold foil to the top of the MWNT films to facilitate heat absorption for measurement purposes [17].

The three-layer heat conduction model, with the silicon substrate assumed to be an infinite medium, was applied to the temperature profile to determine the thermal conductivity of the CNTs. The thermal contact resistance of the gold-CNT interface did not have a significant effect on the calculated thermal conductivity of the CNTs. The effect of the heat loss on the thermal conductivity was negligible since the temperature decay time was only about 400 μs. The average fitted thermal conductivity was reported to be about 15

$\frac{W}{m-K}$. The obtained thermal conductivity values were not dependent upon CNT length. This was attributed to the idea, proposed by Maruyama and verified by Che, that CNT thermal conductivity converges once the CNT length is considerably longer than the phonon mean free path. For this experiment, the phonon mean free path was 20 nm while the MWNT lengths were 10-50 μm. Thus, the thermal conductivity was not a function of CNT length [17].

By comparing the temperature profile of an Au/CNT/Si configuration with an Au/airgap/Si configuration, the effective thermal conductivity of the CNTs was determined using equation 2.1,

$$\frac{K_{tube}}{d} = \frac{K^*_{tube}}{d} + K_{air} \times \frac{1-\delta}{d} \tag{2.1}$$

where K_{tube} was the fitted thermal conductivity of the CNT film, K^*_{tube} was the effective thermal conductivity of the CNTs, K_{air} was the thermal conductivity for air, d was the thickness of the CNT film or airgap, and δ was the volume-filling fraction of CNTs. With an assumed mass density of 1.34 $\frac{g}{cm^3}$ for the MWNTs, the volume-filling fraction was calculated to be around 7-8 % for the four samples used in this experiment. By considering the volume-filling fraction, the CNT film thickness, the thermal conductivity of air, and the fitted thermal conductivity of the CNT film, a thermal conductance model, which used equation 2.1, yielded an effective thermal conductivity of 200 $\frac{W}{m-K}$ for the CNTs [17].

Cola [18] has recently studied the thermal properties of carbon nanotube arrays (CNAs) with vertically-positioned CNTs. Thermal conductivities for these types of CNT configurations have been found to range from 10 to 200 $\frac{W}{m-K}$. An important characteristic of CNT array interfaces is that they are dry and stable in air at extreme temperatures [18].

The effectiveness of CNA TIMs depends on several factors such as array density, array height, CNT diameter, CNT quality, and bonding success to the growth substrate. Thermal resistances were modeled for the CNT-substrate interfaces as well as the array. The array resistance was negligible compared to the CNT-substrate contact resistances when the array

height did not exceed 50 μm. A model that could be used to calculate real contact area indicated a total thermal resistance as low as about 0.1 $\frac{mm^2-K}{W}$ for CNT arrays with a surface density of 108 $\frac{CNTs}{mm^2}$ and 20 nm diameters [18].

Since CNT growth cannot be entirely controlled to obtain all equal nanotube heights, Desai et al. [19] employed an analytical solution and a random number generator to represent different CNT heights to simulate an accurate model for CNAs in contact with an opposing substrate. The corresponding temperature drop for each model system was computed. The analysis looped a specific number of times, and the thermal resistance of each nanotube was recorded. The total effective thermal resistance was determined from the stored values of the individual thermal resistances of the nanotubes. The effective thermal resistance was then used to solve for the effective thermal conductivity of the model TIM layer according to Equation 2.2.

$$K_{eff} = \frac{L}{R_{eff} \times A} \tag{2.2}$$

where K_{eff} was the effective thermal conductivity of the thermal interface layer in $\frac{W}{m-K}$, L was the thermal interface layer thickness in m, R_{eff} was the effective thermal resistance of the thermal interface layer in $\frac{K}{W}$, and A was the area of the TIM layer in squared meters.

Two types of random distributions were used: normal random distribution and uniform random distribution. The normal random distribution assigned the mean value as the average CNT height with a standard deviation of 1 μm. The uniform random distribution produced random numbers that ranged +/- 3 μm from the mean [19].

Two different analyses were used. One analysis assumed nanotubes that were shorter than the mean height had no influence on the effective thermal conductivity. The other analysis did not neglect the effect of the short tubes on the effective thermal conductivity. The four cases that resulted were normal finite, normal infinite, uniform finite, and uniform infinite. Normal finite and normal infinite cases were both normal random distributions, but the effect of the short tubes was only accounted for in the normal finite case. The uniform

finite and uniform infinite cases were both uniform random distributions, but the effect of the short tubes was only accounted for in the uniform finite case [19].

In general, various random distributions along with two separate analyses were utilized to investigate the effect of nanotube height differences on the effective thermal conductivity of the TIM. The results showed the highest thermal conductivity resulted from the normal finite case. Plotting the effective thermal conductivity of the TIM model divided by the bulk thermal conductivity of the TIM model versus the percentage of area covered by CNTs and taking an average of more than six simulations showed that the results would converge into a single line. From the results of this study, it was concluded that TIMs with VACNTs are very promising for applications as high thermal conductivity TIMs in spite of varying nanotube heights [19].

In a study performed by Xu and Fisher [20], CNAs were grown directly on catalyst-coated silicon wafers by microwave plasma-enhanced chemical vapor deposition (PECVD). The silicon wafers were cut into 10 mm $\times$ 10 mm chips. Factors such as size, shape, and chemical composition of the catalysts influenced the resulting CNTs. Nickel and iron were utilized as catalysts for the CNT fabrication process. The configuration of the catalyst structure was titanium-aluminum-iron/nickel. The titanium supported the adhesion to the silicon wafer while the aluminum layer stimulated catalytic activity. The final layer, either nickel or iron, was the catalyst layer from which the CNTs grew. Thermal contact resistances were determined by a reference calorimeter apparatus. All of the interface resistances, as well as the intrinsic resistance of the CNA, were combined for a total thermal interface resistance. The nominal interface temperature stayed around 70°C, and the greatest pressure applied was 0.445 MPa [20].

Four sample types were formed, and their thermal resistances were compared. One of the samples used a nickel catalyst (tilted 75°), another sample used an iron catalyst (tilted 75°), another sample used an iron catalyst with bias (tilted 45°), and the last sample used a nickel catalyst (tilted 49°). A bare wafer was used as a reference. Predictably, the

thermal resistances decreased with increasing pressure. At the highest pressure applied, the thermal resistances of all samples were closely related. For samples 1 through 4, the thermal resistances were 23, 37, 32, and 20 $\frac{mm^2-K}{W}$ (0.23, 0.37, 0.32, and 0.20 $\frac{cm^2-K}{W}$), respectively. The various trends in pressure dependence were attributed to differences in array composition, CNA coverage, CNA heights, area density, and CNT quality [20].

Xu and Fisher [20] previously discovered thermal contact resistances as low as 23 $\frac{mm^2-K}{W}$ (0.23 $\frac{cm^2-K}{W}$) between silicon wafers and copper when a CNA interface was present. In another study, Xu and Fisher [20] compared the thermal resistances of multiple interface configurations. There were six configurations, and three of the configurations included CNTs. A different catalyst configuration (Si-Ti-Al-Ni-CNT) formed by plasma-enhanced chemical vapor deposition (PECVD) improved CNT array height and coverage. CNTs were combined with indium as well as a PCM, and the potential of each combination as a TIM was examined. The resulting thermal resistances were found using a reference calorimeter setup [20].

Copper-silicon interface resistances were compared to copper-CNT-silicon interface resistances at various pressures. The Cu-CNT-Si sample displayed resistances that were all less than 31 $\frac{mm^2-K}{W}$ (0.31 $\frac{cm^2-K}{W}$). The lowest one recorded was 19.8 $\frac{mm^2-K}{W}$ (0.198 $\frac{cm^2-K}{W}$) at 0.445 MPa. It was hypothesized that larger CNA heights would improve the substrate-to-substrate contact by filling the microscopic spaces caused by surface roughness. This theory was based on the fact that a CNA with a height of 7.9 μm showed lower resistances than one with a height of 7 μm. Also, a CNA with a 10 μm height demonstrated lower pressure dependence than shorter array heights. For the given pressure range from 0.169 to 0.445 MPa, the resistance of the taller arrays decreased by 35% , while the shorter ones decreased by 60% [21].

For the Cu-In-Si configuration, interface resistances illustrated a marginal decrease with the addition of the CNA. It was believed that the small improvement may have been because indium filled the interfacial gaps similarly to CNTs. It was also possible that the CNTs and indium did not merge well enough to form a composite material. If this was the case, then

two separate layers with two separate resistances would have existed and hindered thermal conductance [21].

The addition of CNTs to the Cu-PCM-Si compound substantially reduced the thermal resistance. At 0.35 MPa, the lowest resistance recorded was 5.2 $\frac{mm^2-K}{W}$ (0.052 $\frac{cm^2-K}{W}$), while the lowest resistance recorded for the compound without CNTs was 16.2 $\frac{mm^2-K}{W}$ (0.162 $\frac{cm^2-K}{W}$). The PCM layer filled the interfacial gaps more efficiently at pressures higher than 0.28 MPa. Higher pressures also promoted infusion of the CNA and PCM, generating significantly lower resistances [21].

Tong et al. [5] synthesized MWNTs through CVD, using iron as a catalyst. Ion beam sputtering was used to coat the silicon substrate with a 10 nm layer of aluminum and a 10 nm layer of iron. Occasionally, molybdenum was also used as an underlayer to enhance the bond between the MWNTs and the silicon substrate. Thermal conductivity testing was implemented using a phase sensitive transient thermoreflectance technique (PSTTR), established by Ohsone et al. This technique distinguished the phase difference between the heat flux input and the temperature response of the sample [5].

Because of its well-known properties, the silicon wafer was first assessed so that it could be used as a control. For a model calculation, the density and specific heat of silicon was fixed while the thermal conductivity was restricted to a small range. The heat conduction model tested consisted of three layer configuration that consisted of glass-CNT-silicon layers and a heating laser. The MWNTs were 7 μm high, the silicon was 100 μm thick, and the glass was 1 mm thick and coated with a layer of Cr-Au on the inner surface. One of the experiments that did not have a glass layer was used as a reference. One of the other experiments had the three-layer configuration with dry adhesion between the CNTs and glass surface, and the other had the three-layer configuration with the addition of a 1 μm indium layer inserted into the CNT-glass interface. The indium layer was used to thermally weld the CNT free ends to the glass surface [5].

The thermal conductivity of the CNAs varied from 244 to 267 $\frac{W}{m-K}$, and the CNA thicknesses ranged from 4.6 to 10.1 μm. The experiment with dry adhesion revealed a thermal resistance of approximately 0.1111 $\frac{cm^2-K}{W}$ for the glass-CNT interface. The experiment that had its glass-CNT interface bonded with indium resulted in a thermal resistance of approximately 0.00294 $\frac{cm^2-K}{W}$, which was about a 97.4% decrease from the dry interface resistance. The results validate that welding the free ends to the other surface lowers the thermal resistance. Consequently, the thermal conductance at that interface is increased [5].

Various configurations for CNAs include the one-sided CNA interface, the two-sided CNA interface, and the double-sided CNT foil. The one-sided CNA, which is the most commonly researched configuration, involves CNTs grown from a single substrate such as silicon. An opposing substrate can then be brought into contact with the exposed nanotubes. Thermal resistances as low as 7 $\frac{mm^2-K}{W}$ (0.07 $\frac{cm^2-K}{W}$) were revealed experimentally for the one-sided CNA. The two-sided CNA interface involves CNT growth on two substrates. The substrates can then be joined with the separate CNT forests facing each other; this creates a Velcro-like bond. Thermal resistances as low as 4 $\frac{mm^2-K}{W}$ (0.04 $\frac{cm^2-K}{W}$) were revealed experimentally for the two-sided configuration. The double-sided CNT-foil configuration consists of fused CNTs on both sides of a thin foil structure. This structure is convenient for systems where CNTs cannot be grown directly from the devices due to high temperature intolerance of the materials. The CNT-foil structure can simply be inserted into the desired interface. A thermal resistance as low as 8 $\frac{mm^2-K}{W}$ (0.08 $\frac{cm^2-K}{W}$) was found for CNT-coated foil TIMs [18]. Figure 2.1 displayed below shows the various CNA configurations discussed.

Thermal resistances of CNA TIMs have been assessed by some groups through transient methods in order to determine the separate thermal resistances of the different parts of a CNA TIM. These measurements have verified that the contact of the CNT free ends with the opposing substrate produced a much larger thermal resistance than that of the CNT-growth substrate interface, and the CNT-growth substrate interface had a much higher thermal resistance than the intrinsic resistance of the CNA. Since the interfacial contact of the CNT

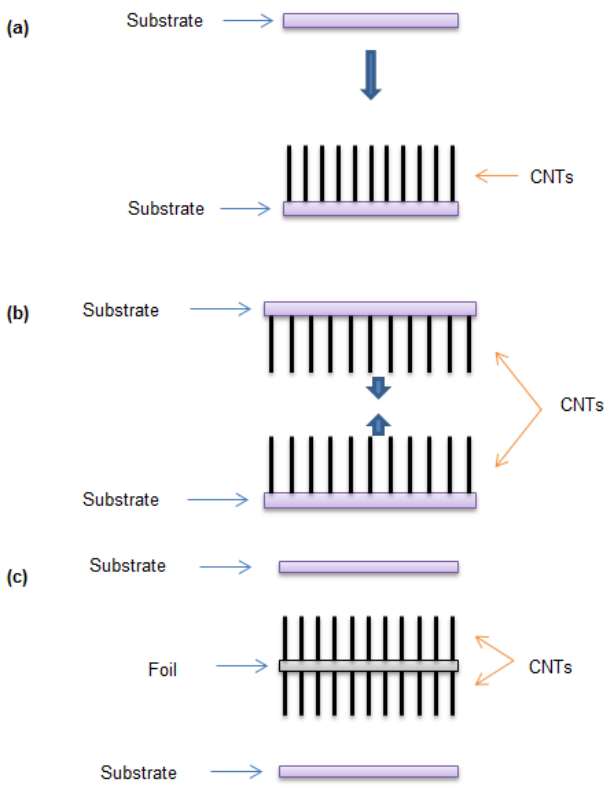

Figure 2.1: Carbon Nanotube Thermal Interface Material Configurations

(a) One-sided carbon nanotube array configuration; (b) Two-sided carbon nanotube array configuration; (c) CNT-foil configuration

free ends with an opposing substrate is one of the major contributors to the thermal resistance in CNA TIMs, bonding the free ends of the CNTs to the opposing substrates was found to generate significantly lower thermal resistances when compared to one-sided CNA interfaces in dry contact with opposing substrates. It has also been found that combining CNAs with TIMs that considerably wet the interface also resulted in lower thermal resistances than that of dry CNA interfaces [18]. Some measured thermal resistance values of various TIM configurations are shown in Table 2.1 and Table 2.2.

An Intel CPU was used to conduct burn-in testing of CNT-coated foil TIMs. The tested TIMs included a 25 μm thick copper foil with CNTs grown on one side. The CNT-coated foil was placed between a die and heat sink in which the CNT free ends were brought in

Table 2.1: Approximate thermal resistance values as a function of pressure for one-sided interfaces

Interface	Average Pressure	Average Thermal Resistance
Bare Si-Cu interface	0.275 MPa	325 $\frac{mm^2K}{W}$
Si-CNT-Cu	0.3 MPa	25 $\frac{mm^2K}{W}$
Si-CNT-Ni	0.3 MPa	16 $\frac{mm^2K}{W}$
Si-CNT-Ag	0.24 MPa	8 $\frac{mm^2K}{W}$

Recreated from Cola [18]

Table 2.2: Approximate thermal resistance values as a function of pressure for two-sided and CNT/foil interfaces

Interface	Average Pressure	Average Thermal Resistance
Bare Si-Cu interface	0.275 MPa	325 $\frac{mm^2K}{W}$
Si-CNT-Cu	0.133 MPa	11.5 $\frac{mm^2K}{W}$
Si-CNT-Ni	0.175-0.375 MPa	4 $\frac{mm^2K}{W}$

Recreated from Cola [18]

contact with a heat sink and the foil was brought in contact with the die. The CNT-coated foils were tested for 1000 thermo-mechanical cycles, and they demonstrated resistances at least 30% lower than those of various bare foil TIMs made from metals such as copper or aluminum. Unvarying performance enhancements were observed for all tested cycles [18].

For some conditions, one or two-sided CNA interfaces are not applicable because the CNTs cannot be easily grown from the substrate surface due to extreme temperatures or surface roughness. Under these circumstances, a CNT-foil TIM can be used. A CNT-foil TIM is fabricated by growing CNTs on both sides of a metal foil. Aside from overcoming the previously stated issues, foil deformation aids in filling the interface gap by increasing the amount of contact points between the exposed CNT free ends and the opposing substrate. This type of TIM can be inserted into various interface arrangements like other high-quality TIMs. Another advantage of a CNT-foil TIM is that it is dry, removable, and possesses an inherently high thermal conductivity [2].

The performance of CNT-foil TIMs is dependent on the metal properties of the foil, which affect the interfacial thermal resistance, the CNT array characteristics such as the density of CNTs and nanotube diameter, and the quality of the bond between the CNTs and foil. Past studies have revealed CNAs to have effective thermal conductivities of approximately 80 $\frac{W}{m-K}$. Their ability to adapt between interfaces exceptionally has also been established. The properties of CNAs and metal foils can be modified to fill interface gaps efficiently; therefore, significant improvements in interfacial thermal resistance can be achieved with suitable manipulation [2].

In a study performed by Cola et al. [2], CNTs were fabricated through PECVD. The catalyst layer configuration that was deposited on both sides of a 10 μm thick copper foil consisted of 30 nm titanium, 10 nm aluminum, and 3 nm iron. H_2 and CH_4 were used as process gases. A temperature of 900°C and pressure of 10 Torr were used for the CNT growth conditions. The resulting CNT-foil had CNAs of around 50 μm tall with diameters of approximately 20 nm. The CNA density was reported to be around 10^8 $\frac{CNTs}{mm^2}$ [2]. An SEM image of the fabricated CNT-foil TIM is shown in Figure 2.2. The CNT coverage percentage was calculated by the following steps shown in Equations 2.3 through 2.6.

Since the CNT diameter is 20 nm or 2×10^{-5} mm,

$$\frac{area}{CNT} = \frac{\Pi}{4} \times (2 \times 10^{-5}\, mm)^2 \tag{2.3}$$

$$\frac{area}{CNT} = 3.1416 \times 10^{-10}\, mm^2 \tag{2.4}$$

Since the CNA density was 10^8 $\frac{CNTs}{mm^2}$,

$$10^8\, \frac{CNTs}{mm^2} \times (3.1416 \times 10^{-10}\, mm^2) = 0.0314 \tag{2.5}$$

$$\%\, coverage = 3.14\% \tag{2.6}$$

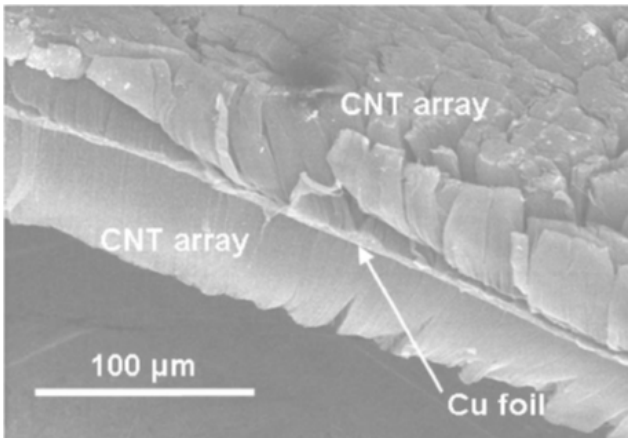

Figure 2.2: CNT Array on Copper Foil

Using a photoacoustic (PA) technique, the thermal resistances of the produced CNT-foils were compared to those of a 10 μm thick Cu foil over a range of pressures. The results of the interfacial thermal resistances of the bare foil and CNT-coated foil are displayed in Figure 2.3. Both types of TIMs displayed rather low thermal resistances due to the mostly smooth interface surfaces, which may have left little room for improvement. Nevertheless, the CNT-foils proved to have lower thermal resistances than that of the bare foils. At 275 kPa, the CNT-foil resistance was about 30% lower (about 13 $\frac{mm^2-K}{W}$) than the bare foil interfacial resistance in the copper-silver interface, and the CNT-foil interfacial resistance was about 15% lower (about 8 $\frac{mm^2-K}{W}$) than the bare foil interfacial resistance in the silicon-silver interface. The more significant decrease in thermal resistance in the copper-silver interface was attributed to greater surface roughness that may have hindered the CNTs from filling the gap at lower pressures. A thermal resistance of 4 $\frac{mm^2-K}{W}$ (0.04 $\frac{cm^2-K}{W}$) was calculated as the total resistance of the CNT-foil material, which was comprised of the Cu foil, the CNT-foil interfaces, and the CNT arrays. The remaining thermal resistance was attributed to the CNT free ends and the CNT-substrate interfaces. Figure 2.4 shows a more detailed analysis of the thermal resistance network shown in Figure 2.5, which was completed by examining the local component resistances. When the thermal resistances of the free surfaces of the bare foil samples were compared to those of the CNT-foil samples, more than a 50% decrease

in thermal resistance was perceived. The free surface resistance for the CNT-foils was the sum of the interface resistances of the two exposed CNT tip surfaces [2].

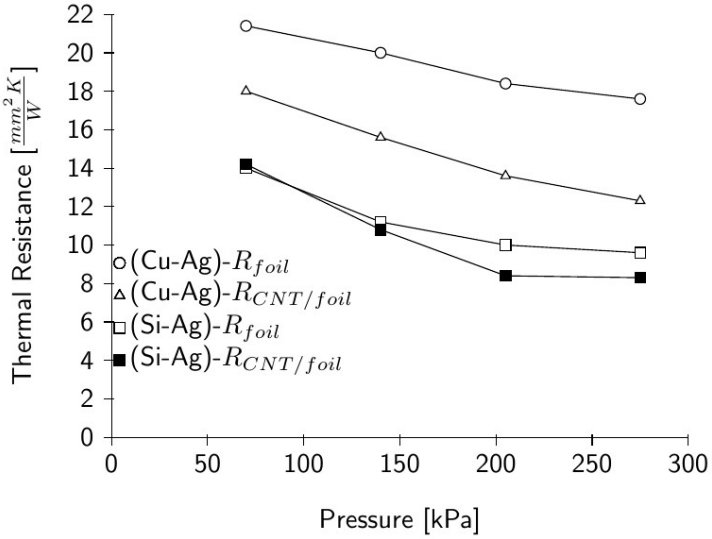

Figure 2.3: Thermal Resistances of Bare Foils and CNT-coated Foils as a Function of Pressure recreated from Cola et al. [2]

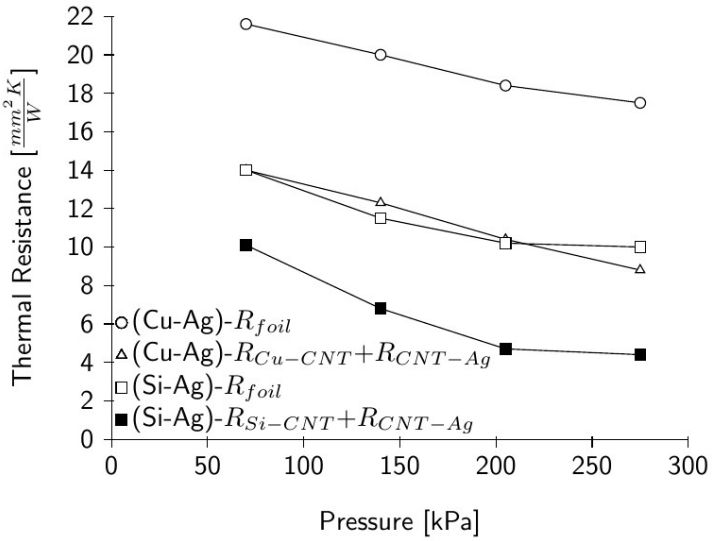

Figure 2.4: Thermal Resistances of Local Components in Foil TIMs as a Function of Pressure recreated from Cola et al. [2]

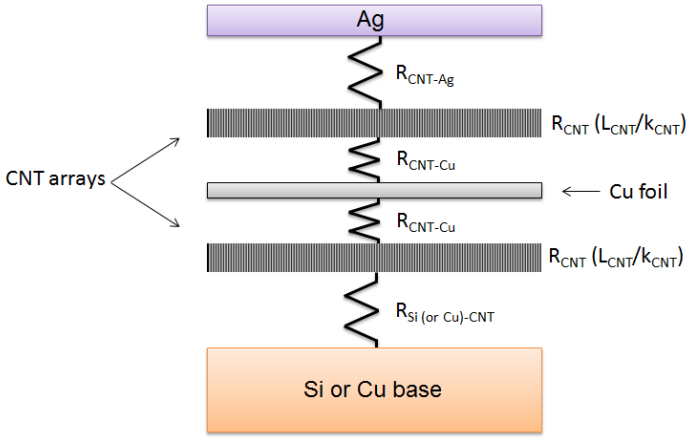

Figure 2.5: Thermal Resistance Network of CNT/Foil TIM recreated from Cola et al. [2]

The effectiveness of the CNT-foil configuration can be accredited to both the deformation of the foil and the deformation of the nanotubes. The distortion of these materials assists in increasing the quantity of contact points at the interface, resulting in lower thermal resistances. Cola et al. hypothesized that the CNT deformation was elastic since no tube buckling was observed. To optimize thermal resistance values, the CNT-foil TIM should be chosen for the specific interface and application [2].

One issue with using CNAs for TIM applications is that the free ends of CNTs increase the thermal resistance at the interface. Wu et al. [22] sought to improve the thermal resistance contributed by the nanotube tips by adding a continuous 1 μm thick aluminum layer to a CNA via electron beam evaporation. To preserve the CNA during testing, a plastic film was placed on the CNA to create a protective layer while a silicon rubber called polydimethylsiloxane (PDMS) was inserted into the medium to support the CNA. The PDMS was cured with tetraethyl silicate, forming a gel medium within the CNA. After the new composite was molded, the plastic layer and substrate were easily removed. Any remaining residues were rinsed off with xylene. The CNA structures were cut into 8 mm $\times$ 10 mm pieces, and their thermal conductivity was measured with a device using the ASTM D5470 methods [22].

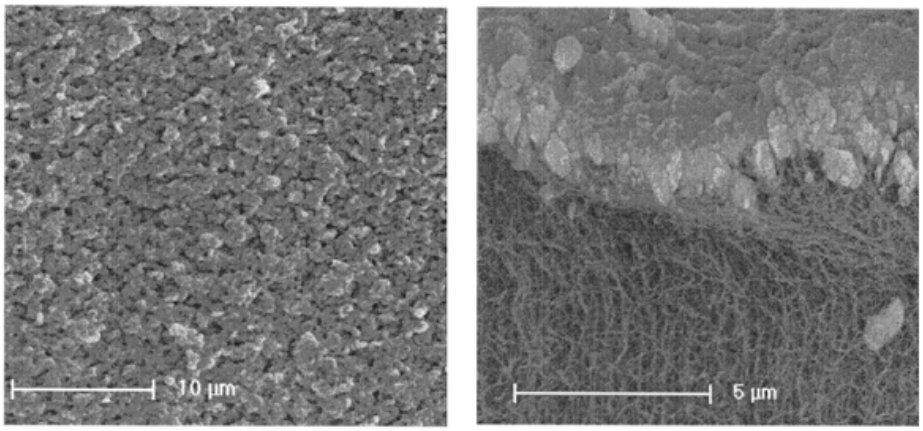

Figure 2.6: SEM of Aluminum-coated Carbon Nanotube Array

Left: Bird's eye view of aluminum-coated CNA borrowed from Wu et al. [22]; Right: Side view of aluminum-coated CNA borrowed from Wu et al. [22].

CNA samples with an aluminum layer, which can be seen in Figure 2.6, were compared to those without a metal layer. The thermal resistance was significantly reduced by approximately 50% with the addition of an aluminum layer. Plotting the resulting thermal resistance values against the sample thicknesses revealed parallel lines, which confirms that the intrinsic thermal conductivities corresponded well. The aluminum layer produced a heat current collector that facilitated thermal conduction and lowered the thermal resistance. An aluminum layer coating further enhanced performance by interconnecting the CNT tips that may have otherwise tangled amongst each other or become embedded inside the CNA. Significantly lower thermal resistances could have likely been achieved if an aluminum layer was added to both sides of the CNA [22].

The results demonstrated an intrinsic thermal conductivity of approximately 0.43 $\frac{W}{m-K}$, which was three times the conductivity of a pure PDMS matrix at 0.11 $\frac{W}{m-K}$. The low thermal conductivity values reported were credited to the low weight percentage of CNTs (approximately 0.3 wt%). Phonon scattering between the CNTs and polymer molecule was another factor that may have lowered thermal conductivities due to impedance of phonon conduction [22].

Table 2.3: Best-fit Values for Metallized Single-Walled Carbon Nanotube Film recreated from Hu et al. [3]

Parameter	Average Result	Uncertainty (%)
$C_{CNT,eff}$	5.2 kJ $m^{-3}K^{-1}$	12%
$R''_{CNT-Pd,eff}$	2.9 $m^2K^1MW^{W-1}$	21%
$R''_{CNT-SiO_2,eff}$	9.1 $m^2K^1MW^{W-1}$	31%
$K_{CNT,eff}$	>8 $Wm^{-1}K^{-1}$	n/a

Hu et al. [3] assessed the room-temperature thermal properties of an aluminum-coated CNA with a nanosecond thermoreflectance technique. To fabricate the sample, an iron film was deposited on a 10 nm thermal oxide layer of a silicon substrate. Iron clusters were formed through annealing at 550°C and were used as catalyst sites for CNT growth through coupled-rf CVD. A 20 nm palladium layer was incorporated on the free ends of the 28 μm thick SWNT film for adhesion. Subsequently, a 160 nm layer of aluminum was evaporated onto the palladium layer for measurement purposes. The surface roughness of the film, determined through atomic force microscopy (AFM), was estimated to be approximately 60 nm [3].

Nine different measurements at various sample locations and laser pump powers were taken to generate averages for CNT heat capacity, CNT-Pd interfacial thermal resistances, CNT-SiO2 interfacial thermal resistances, and CNT effective thermal conductivities. The results for the average best-fit values for the 28 μm thick sample with the $Si - SiO_2 - SWNT - Pd - Al$ configuration are summarized in Table 2.3. It was concluded that the interfacial thermal resistances were higher than expected due to topography effects. Out of about 12% true volume fraction, only about 0.35 vol% actually aided in thermal transport [3].

One of the issues concerning the use of CNT films as TIMs includes the extremely high temperatures that are needed for CNT fabrication since those temperatures do not allow for direct synthesis on electronic packaging systems. Another concern is the weak adhesion between the CNTs and their original substrate. Not only does the poor bond between

the CNTs and growth substrate contribute significantly to the thermal resistance at that interface, but it also affects long-term functionality. Zhu et al. [23] focused on resolving this problem by developing a CNT transfer process in their study, which was dubbed "CNT Transfer Technology" [23].

To construct the CNT film samples, silicon wafers were first coated with SiO_2 by thermal oxidation. Al_2O_3/Fe catalyst layers were then e-beam evaporated onto the silicon wafer, and CVD (at 700°C for 10 minutes) was used to grow open-ended nanotubes. Spatially resolved energy-dispersive X-ray spectroscopy was applied to analyze CNT purity and the catalyst layer at various locations [23].

The produced open-ended nanotubes were transferred to copper substrates that had a layer of stencil-printed eutectic tin-lead paste. First, the silicon-CNT substrates were flipped so that the CNT tips were contacting the Cu-Sn/Pb assembly. Then, the assembly was reflowed in a seven-zone reflow oven at a peak temperature of 250°C to form electrical and mechanical contacts. Lastly, the original silicon substrate was removed. The adhesion between the CNTs and the copper substrate was tested by pulling a section of CNTs away from the surface with tweezers. The CNTs broke along their axis and not from the CNT-Cu interface, exhibiting effective bonding between the nanotubes and the new copper substrate [23].

The nanotube film height was recorded to be approximately 180 μm. Thermal measurements revealed a thermal conductivity of 81 $\frac{W}{m-K}$ and a thermal resistance of 0.43 $\frac{cm^2-K}{W}$. The higher than expected thermal resistance value was attributed to the CNT quality and solder layer thickness. Open-ended CNT arrays are fundamental for successful CNT transfer to other substrates through a solder reflow process. "CNT transfer technology" solves the temperature compatibility issue related to using CNTs as TIMs by allowing the transfer of CNTs to other substrates that are not compatible with the high temperatures needed to grow CNTs [23].

In another CNT transfer experiment performed by Barako et al. [24], nanotubes were grown on silicon substrates and transferred using one of two kinds of binder metal layers. The binder metal layer improves the thermal conductance at the CNT-device interface without damaging the inherent thermal conductivity of the CNT film. The two types of metal binder layers that were investigated were an indium thin film binder and a commercial Al/Ni film also known as a Nanofoil. For each experiment, the CNT film thermal conductivity, the interfacial thermal resistances before and after bonding, and the thermal properties at different compressive strains were measured [24].

The CNTs were grown on the silicon wafers through CVD. The generated CNTs had a film thickness of 500 μm, an inner diameter of 5-8 nm, an outer diameter of 7-10 nm, and a film density of approximately 1010-1011 $\frac{CNTs}{cm^2}$. Fused silica substrates that were used as the opposing substrates and the CNT films were layered with 50 nm chromium, 20 nm nickel, and 150 nm gold via electron beam evaporation. The gold layer was used as a bonding layer to weld the solder layer, the nickel layer was used to block the diffusion of gold atoms, and the chromium layer was an adhesion layer [24].

For the experiment with the indium metal binder layer, a 25 μm thick indium foil was used. The foil was inserted between the CNT film and the fused silica (FS) substrate. The FS substrates were later used as reference layers during thermal measurements since FS has a steady thermal conductivity over a large temperature range. The assembly was heated on a hot plate at 180°C with approximately 100 kPa of applied pressure to promote effective contact and wetting. The experiment using the Al/Ni film (Nanofoil) bonding layer underwent the same preparation but used a different bonding process. The Nanofoil was inserted in the interface and ignited to start an exothermic reaction that melted the Sn-plating and bonded the two gold layers. The resulting Sn-Au bond was stable up to 1000°C [24].

The thermal conductivities and thermal resistances of the samples were measured with comparative infrared microscopy. The CNT-In-FS thermal boundary resistance, which varied

with pressure, was recorded to be 28-71 $\frac{mm^2-K}{W}$ (0.28-0.71 $\frac{cm^2-K}{W}$). When comparing the dry interfacial thermal resistances to the bonded interfacial thermal resistances, it was found that the interfacial resistance decreased from about 1000 $\frac{mm^2-K}{W}$ to approximately 50 $\frac{mm^2-K}{W}$ (10 $\frac{cm^2-K}{W}$ to 0.5 $\frac{cm^2-K}{W}$). These results were strongly dependent on indium wetting. For the Nanofoil bonding, the dry thermal resistance was measured to be approximately 1000 $\frac{mm^2-K}{W}$ (10 $\frac{cm^2-K}{W}$), and the bonded thermal resistance ranged from 15-50 $\frac{mm^2-K}{W}$ (0.15-0.5 $\frac{cm^2-K}{W}$) [24].

Since the metal layer bond strength was greater than the van der Waals forces between the CNTs and silicon substrate, the silicon substrate was easily removed and another substrate could be bonded to the bare CNT surface [24].

Cross et al. [25] grew VACNTs with lengths of 20-225 μm via CVD. Both one-sided CNA samples and transfer-printed samples were constructed. The one-sided CNA, which was previously mentioned, involved growing CNTs on a desired substrate. In this configuration, the CNTs are exposed and can be brought into dry or bonded contact with an opposing substrate. For the transfer-printed samples, copper substrates and the nanotube free ends were metallized with 50 nm titanium and 500-1000 nm of Au. The Au-Au interface bonded through self-diffusion of Au rather than a reflow process. An external load is typically applied to aid in this type of bonding. In this study, a Carver benchtop hot press at 220°C was used to bond the metallized surfaces. Complete nanotube transfer occurred for samples that underwent water vapor etching. The original substrate was removed for these samples and another substrate was bonded to the exposed nanotubes, allowing them to operate as die attachment material [25].

Tensile strength tests were performed on the samples that were bonded to copper substrates (Si-CNT-Cu). Good bond strength was observed. Failure happened at loads from 35 to 40 $\frac{N}{cm^2}$. Thermal resistances of 0.045 $\frac{cm^2-K}{W}$ and 0.1 $\frac{cm^2-K}{W}$ were measured for the one-sided samples and transfer-printed samples, respectively. These values were found to be independent of CNT height. Another detail that should be noted was that the thermal

resistance of the one-sided sample was about half of the thermal resistance of the sample with two interfaces. Accordingly, it was concluded that the interfacial resistance was the main contributor in the overall thermal resistance [25].

Because of recent developments in the electronics industry such as using lead-free solders and including a large amount of circuits on a single chip, reliability concerns for electronic components have surfaced. Previous reliability assessment techniques may no longer be valid since the parameters of a lead-containing system are substantially different from those of a lead-free system. Solder joint reliability in electronic packaging is fundamental to long-term reliability of microelectronic components since solder joints are the usually the only mechanical attachment for electronic components to the printed circuit board (PCB). Solder joints in electronic packaging undergo thermal cycling, which causes expansion of both the solder joints and other components. There is often a coefficient of thermal expansion (CTE) disparity between the solder and packaging components. Consequently, the solder joints are constrained during thermal changes, which ultimately results in solder joint failure. CTE mismatches between solder and packaging components are even more crucial as operating temperatures increase [26].

Shang et al. [26] conducted an experiment to analyze long-term reliability in ball grid array (BGA) packages using Moire interferometry, which includes high frequency grating techniques as well as laser interferometry. Three groups of samples were subjected to thermal cycling. There were four samples in each group, and each sample had a 256 BGA sample mounted to a PCB. The first two groups had similar parameters, but one group used lead-free solder while the other used a lead-containing solder. The third group included samples that comprised a lead-containing solder with different size parameters than the first two groups. The samples underwent thermal cycling tests in a thermal cycling loading chamber. The tests were completed for a temperature range between room temperature and 125°C using a resistance heater as the heat source.

Shear concentrations were observed at the tri-material corner where the silicon, solder, and pad came in contact. The highest shear strain was seen for the solder joint located beneath the corner of the silicon chip. In comparison with the other solder joints, the corner solder joint was expected to have the shortest service life. Others have also reported that failure is expected at the corner solder joints [14]. Shang et al. [26] also observed that shear strain decreased with increasing solder height. For example, a 21 percent decrease in shear strain was seen at 125°C when solder height was increased from 0.6 mm to 0.8 mm. Furthermore, this study concluded that the predicted life of BGA packages decreased as solder height decreased [26].

The previous literature discussed TIMs, thermal properties of CNTs, various configurations of CNT arrays, thermal performance of CNA TIMs, and ways thermal performance of CNA TIMs could be enhanced. Solder joint reliability concerns in electronic packaging were also discussed, and an experiment involving the effects of thermal cycling on different types of solder joints was reviewed. The focus of the following work was to fabricate a CNA TIM that overcame issues such as high interfacial thermal resistances between the growth substrate and CNTs and between the CNT free ends and the opposing substrate as well as issues related to coefficient of thermal expansion (CTE) mismatches in solder joints. Additionally, the need for high quality CNTs as well as densely packed CNT arrays was taken into account. Accordingly, a CNA TIM was constructed through a CNT transfer process where good quality CNTs, which were grown on a silicon substrate, were transferred and soldered to a copper disk on both sides of a CNT array. The goal of this work was to create a CNA TIM that displayed low thermal resistances, surpassed the thermal performance of commercially available TIMs, and structurally-enhanced the solder joint.

Chapter 3

Fabrication

Chemical vapor deposition (CVD), a process in which a hydrocarbon vapor is thermally decomposed in the presence of one or more metal catalysts, is the most common method for fabricating carbon nanotube arrays (CNAs). CVD fabrication offers several advantages over other fabrication methods such as arc-discharge and laser-ablation. While arc-discharge and laser-ablation generally offer better crystallinity, CVD is a superior method for CNT yield and purity. CVD is a fairly simple and economical process. Additionally, CVD fabrication offers versatility by allowing the use of different growth substrates, and it also allows CNT growth in various forms including powder, thin films, and patterned CNTs. Essentially, CVD permits manipulation of its growth parameters in numerous ways [27].

In general, CVD passes a hydrocarbon vapor through a cylindrical reactor that contains a catalyst material at a high temperature, usually ranging from 600°C to 1200°C. The hydrocarbon vapor contacts the hot metal and decomposes into hydrogen and carbon. While the hydrogen floats away, the carbon dissolves into the metal. Eventually, the metal's carbon-solubility limit is attained, resulting in the precipitation and crystallization of carbon in a tubular arrangement. Since the hydrocarbon decomposition is an exothermic process and the carbon crystallization is an endothermic process, the existing thermal gradient maintains the process [27].

The main parameters that affect the characteristics of grown CNTs are the CNT precursors, CNT catalysts, and CNT catalyst supports. The CNT precursor is the hydrocarbon containing vapor. While there are numerous precursors available, common CNT precursors include methane, ethylene, and benzene. Ever since Maruyama et al. reported the synthesis of high-purity single-walled carbon nanotubes (SWNTs) using ethanol as a precursor in

2002, alcohol became the most prevalent precursor for CVD-grown CNTs. One important benefit of using an ethanol precursor to grow CNTs is the very low amounts of amorphous carbon produced. The structure of synthesized CNTs is directly affected by the precursor's molecular structure. For example, linear hydrocarbons typically generate straight, hollow CNTs, while cyclic hydrocarbons produce curved or hunched nanotubes. It is essential to choose the appropriate CNT precursor and vapor pressure because both of these parameters influence the duration of the catalyst and the CNT growth rate, which ultimately affect CNT yield and quality. CNT catalysts, or the metal particles which allow the decomposition of hydrocarbons at lower temperatures, influence the properties of the fabricated CNTs in numerous ways. Fe, Co, and Ni metals are frequently used as catalysts since there is a high carbon diffusion rate and high carbon solubility at elevated temperatures in these metals. These commonly used metals also provide a substantial temperature range for the CVD process for various carbon precursors. It is also believed that Fe, Co, and Ni catalysts may form a better bond with the grown nanotubes. The particle size of the catalyst controls nanotube diameter. The particle size can also determine whether SWNTs or MWNTs form. SWNTs typically develop when the particle sizes are only a few nm, and MWNTs form when particle sizes are several tens of nanometers wide. Thus, the diameter of grown CNTs can be regulated by selecting metal nanoparticles of a particular size, and uniform CNT growth can be achieved by depositing catalyst thin films on growth substrates. The CNT catalyst support material is also termed the growth substrate. Because catalysts behave differently on different growth substrates, it is important to assess the catalyst-substrate interaction in order to effectively synthesize CNTs. The surface morphology and texture of the growth substrate also have an effect on CNT quality and yield. Other considerations for CVD-grown nanotubes include the process temperature, pressure, gas-flow rate, deposition time, and reactor geometry [27].

Growing nanotubes through CVD requires that the hydrocarbon be decomposed only on the metal surface. The thermal decomposition involved in CVD, known as pyrolysis, can be

controlled by choosing the appropriate hydrocarbon, catalysts, catalyst concentration, vapor pressure, and reaction temperature. As previously mentioned, iron is commonly used as a catalyst for CVD-grown nanotubes because of its ability to produce a high yield of CNTs. Unfortunately, it produces poorly-graphitized CNTs. Conversely, cobalt catalysts are able to generate well-graphitized CNTs, but the amount of CNT deposits is lower compared to iron catalysts. Accordingly, a combination of iron and cobalt was attempted, and the combination successfully overcame the previously discussed issues to produce a high quantity of well-graphitized MWNTs. Since the melting point of the iron/cobalt combination was lower than their separate melting points, CNTs were able to be fabricated at a lower temperature of 550°C. Metal alloys are recognized as superior catalysts to pure metals. Another key parameter for CVD is the concentration of the catalyst. The catalyst concentration determines whether SWNTs or MWNTs grow or whether CNTs grow at all. In a particular experiment using zeolite, conducted by Kumar and Ando [27], it was observed that no CNTs grew when the weight percent of zeolite was less than 2.4%. Lower weight percentages of 2.4 to 5% resulted in SWNT growth, and higher weight percentages typically resulted in MWNT development. The vapor pressure of a CVD process that uses gaseous hydrocarbons can be managed by adjusting the gas-flow rate and using a rotary pump for suction. The reaction temperature used in CVD is another important consideration because it not only affects CNT diameter, but it also affects whether SWNTs and MWNTs are synthesized. In particular, higher growth temperatures result in larger CNT diameters. Additionally, Kumar and Ando [27] observed that quality CNTs, possessing negligible amounts of metallic impurity, grew in temperatures of up to 750°C. At temperatures higher than 750°C, the range of diameter-distribution was observed to greatly increase. Temperatures of 850°C and higher demonstrated SWNT growth among MWNTs. The fabrication of MWNTs and SWNTs can be controlled with the CVD reaction temperature as well as the catalyst concentration [27].

The commercialization of CVD-grown nanotubes encounters several issues. One of these issues is that scaling up the CVD process results in less control of CNT properties than when

CNTs are synthesized in small reactors. Therefore, CNT purity decreases while the diameter-distribution of the nanotubes increases. Another possible issue related to CNT production that has been cited is the decrease of fossil fuels such as methane, acetylene, and benzene, which are often used in CNT technology. In order to mass produce CNTs, a more precise method for engineering CNTs and dependable renewable resources that can be used as CNT precursors should be examined [27].

3.0.1 Sample Preparation

Vertically-aligned carbon nanotube arrays (VACNAs) were ordered from NanoLab Inc., a manufacturing company headquartered in Waltham, Massachusetts. NanoLab produces carbon nanotubes (CNTs) and nanoscale devices. The VACNAs were grown on a 33 mm $\times$ 33 mm silicon substrate and were fabricated in a manner that would allow easy separation from the growth substrate. The CNT array thickness was between 20 and 100 μm, and the thickness of the growth substrate was 625 μm.

There are several methods that can be used to examine the quality of CNTs. Some of these methods include scanning electron microscopy (SEM), transmission electron microscopy (TEM), and Raman spectroscopy. Quantitative features such as CNT diameter and interlayer spacing can be determined by some customary microscopy methods, such as TEM. Additionally, these techniques enable a better understanding of nanotube purity qualitatively. In Raman spectroscopy, there are three characteristic peaks of multi-walled carbon nanotubes (MWNTs) known as the D-band, the G-band, and the G'-band. The D-band peak, which occurs at a wavenumber around 1350 cm^{-1}, is representative of MWNT defects such as carbonaceous impurities and broken sidewall bonds. The G-band, occurring around a wavenumber of 1580 cm^{-1}, arises according to the graphitic quality of the sample such as crystallinity. The G'-band is characteristic of long-range order in a sample. Raman spectroscopy has conventionally measured CNT purity by calculating the ratio of the D-band peak to the G-band peak [28].

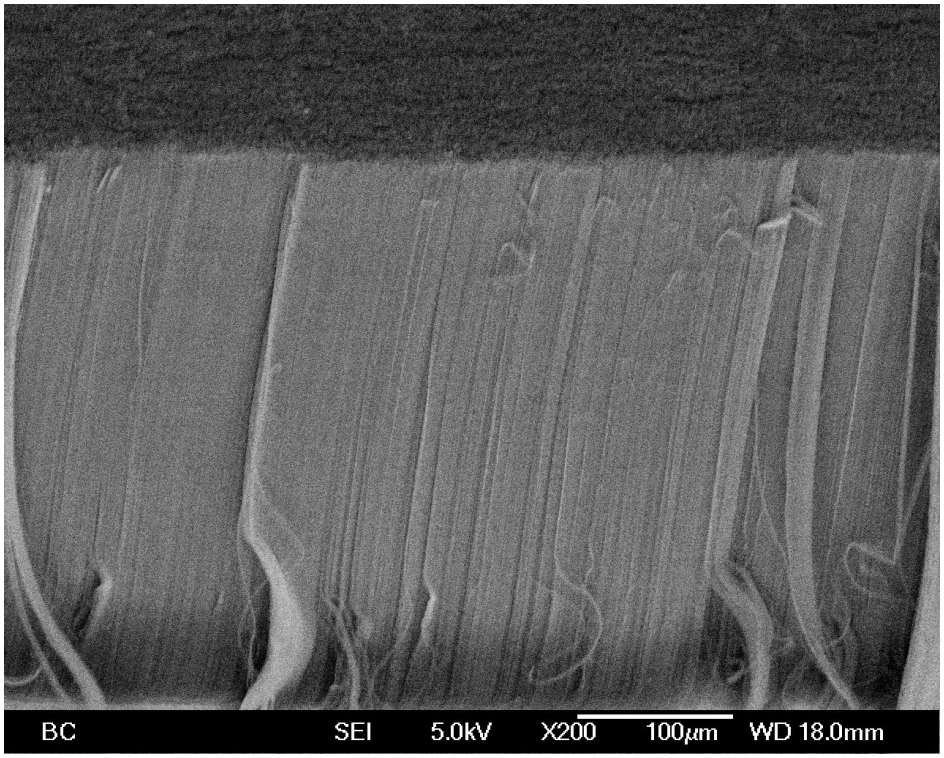

Figure 3.1: SEM of Vertically-Aligned Carbon Nanotubes provided by NanoLab Inc.

Scanning electron microscopy (SEM) and Raman spectroscopy images for the ordered VACNA samples were provided and can be seen in Figure 3.1, Figure 3.2, Figure 3.3, and Figure 3.4. Figures 3.1, 3.2, and 3.3 show side views of the VACNA sample.

Figure 3.4 shows a Raman spectroscopy image that is representative of the VACNA used in this research. The incorporated VACNAs were grown at an approximate temperature of 735°C. As previously mentioned, the G-peak indicates the honeycomb structure of CNTs, while the D-peak symbolizes the disorder that exists in the honeycomb structure. The Raman data shown is consistent with CNTs synthesized by NanoLab. The x-axis represents the wavenumber in cm^{-1}, and the y-axis denotes the relative intensity. The ratio of the highest peak of the D-band intensity to the highest peak of the G-band intensity allows CNTs to be analyzed for various applications. D to G ratios in the range from 1 to 5 are common among MWNTs. The Raman graph shown in Figure 3.4 reveals D to G ratios of approximately 1.5 and 2.3, which corresponds to the expected ratio range for MWNTs.

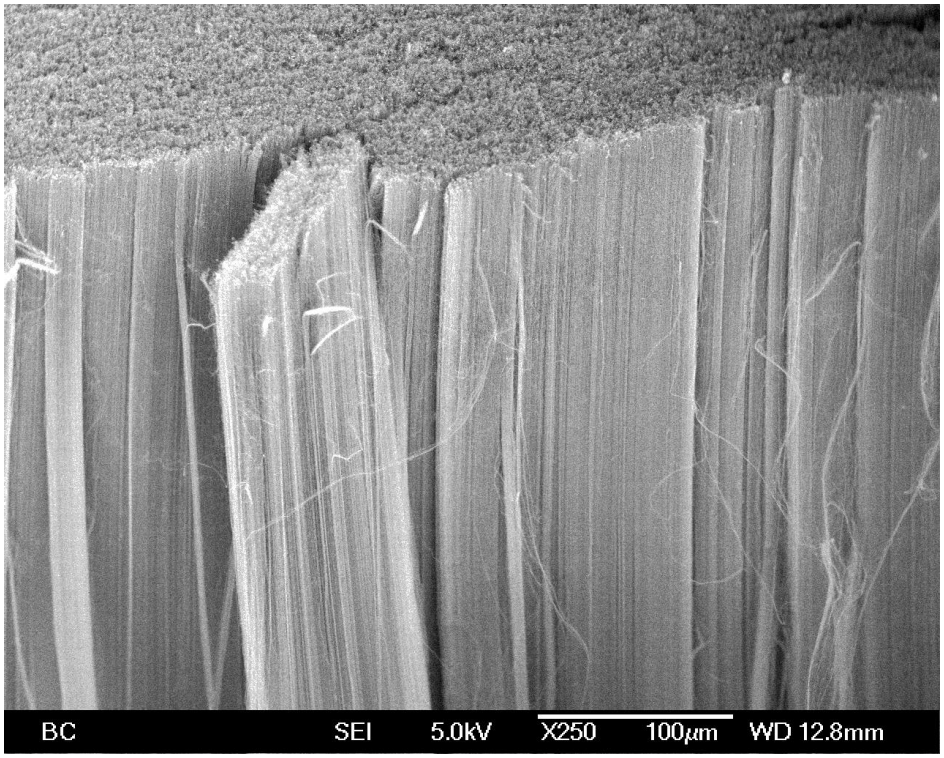

Figure 3.2: SEM of Vertically-Aligned Carbon Nanotubes provided by NanoLab Inc.

The exposed CNT ends of the VACNA sample underwent electron beaming to deposit a 500 angstrom layer of titanium, a 2000 angstrom layer of nickel, and a 500 angstrom of gold, which is shown in Figure 3.5. The Ti/Ni/Au layer configuration was then soldered to a 33 mm diameter Alloy 110 copper disk in a Thermcraft vacuum furnace, which can be seen in Figure 3.6 and Figure 3.7, using Indium Corp. Indalloy 282 57Bi/42Sn/1Ag Lead-Free Solder Alloy. To remove the silicon growth substrate, the sample was soaked in a hydrofluoric (HF) acid bath for 20 hours. The HF solution had a concentration of 48% and was diluted in deionized water to a ratio of 4:100. The HF solution broke the bond between the silicon substrate and CNTs by dissolving the silicon dioxide layer that existed between the CNTs and the surface of the silicon substrate. Because HF is chemically inert, the properties of the CNT are expected to be unaffected [29]. The newly exposed CNTs tips were electron beamed with the same Ti/Ni/Au configuration and soldered to a similar copper disk using the previously mentioned process. The resulting sample configuration

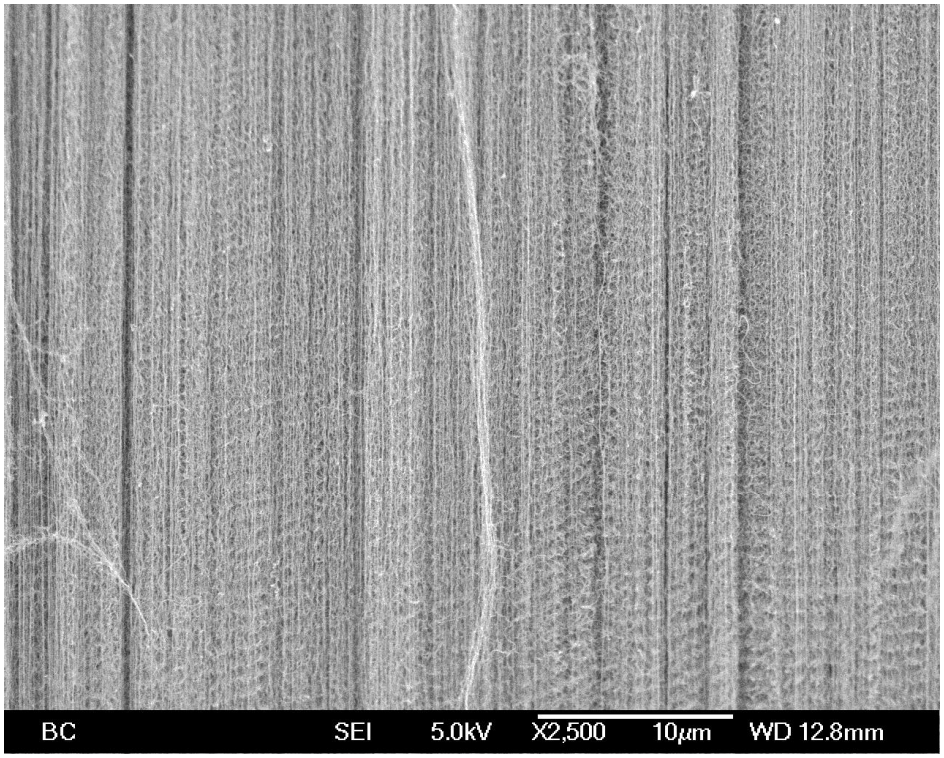

Figure 3.3: SEM of Vertically-Aligned Carbon Nanotubes provided by NanoLab Inc.

was copper disk-Bi/Sn/Ag solder-Ti/Ni/Au-CNTs-Ti/Ni/Au-Bi/Sn/Ag solder-copper disk, shown in Figure 3.8. The thermal properties of the constructed sample were tested with a Thermal Interface Material Tester (TIM tester). The testing methodology will be explained subsequently.

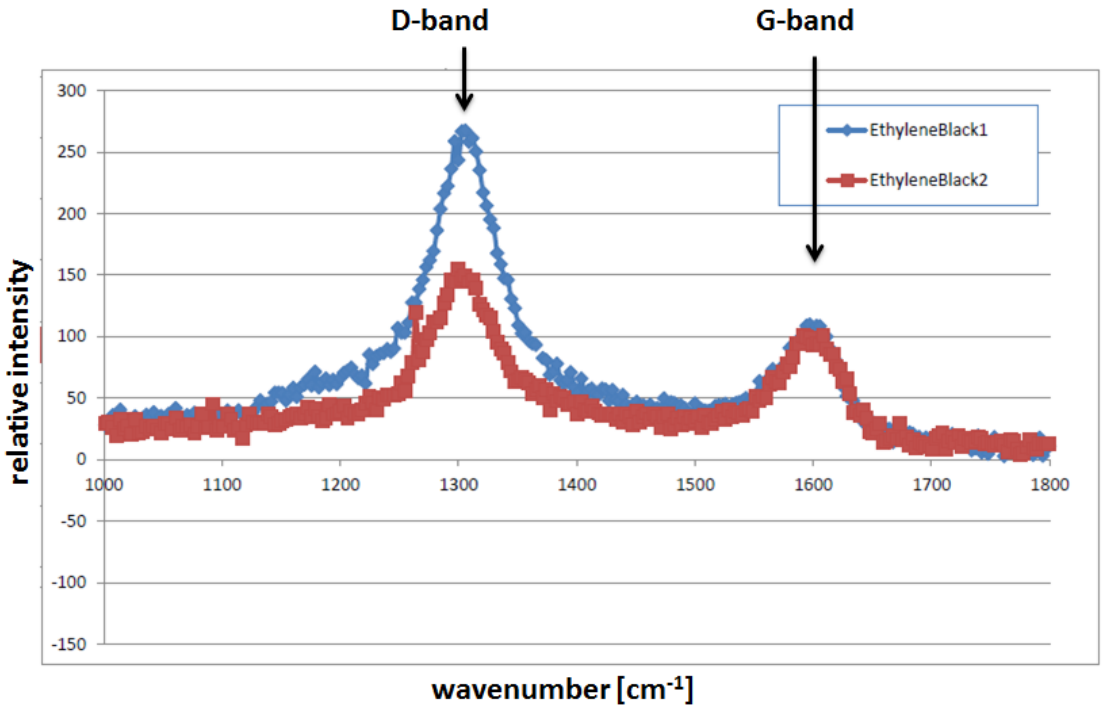

Figure 3.4: Raman Spectroscopy of Vertically-Aligned Multi-walled Carbon Nanotubes

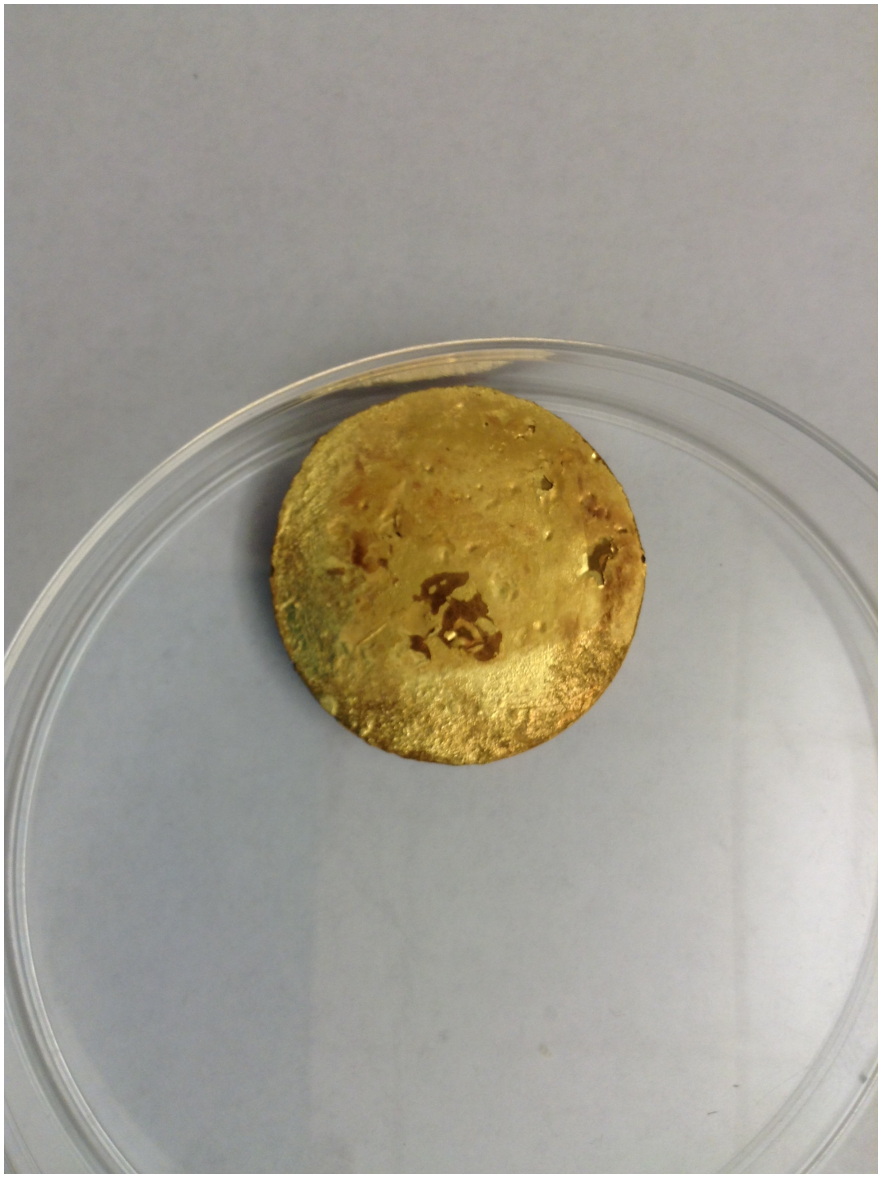

Figure 3.5: E-beamed Layers on Copper-CNT Disk Sample

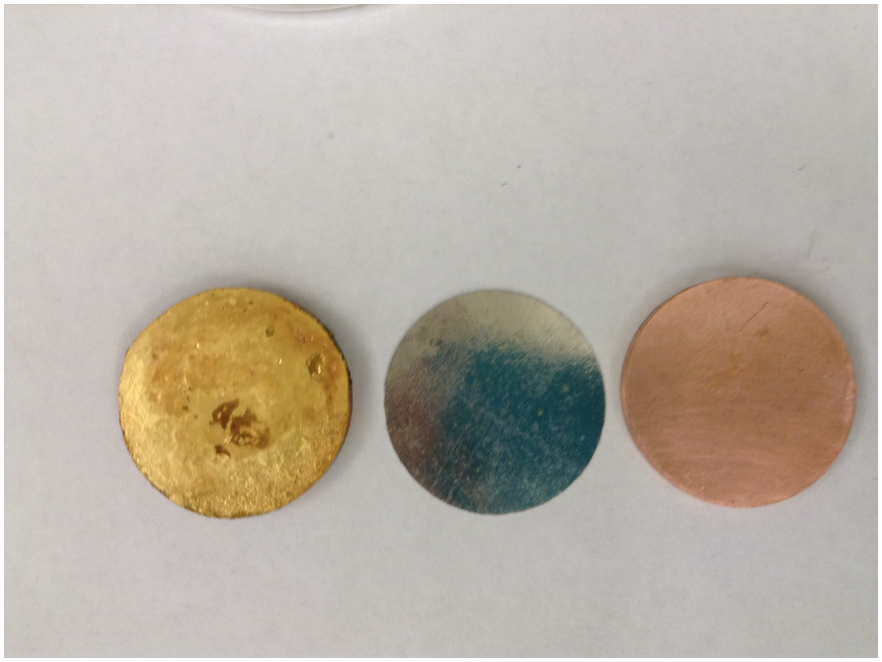

Figure 3.6: Copper-CNT, Bismuth-Tin-Ag Solder, and Copper Disk Sample

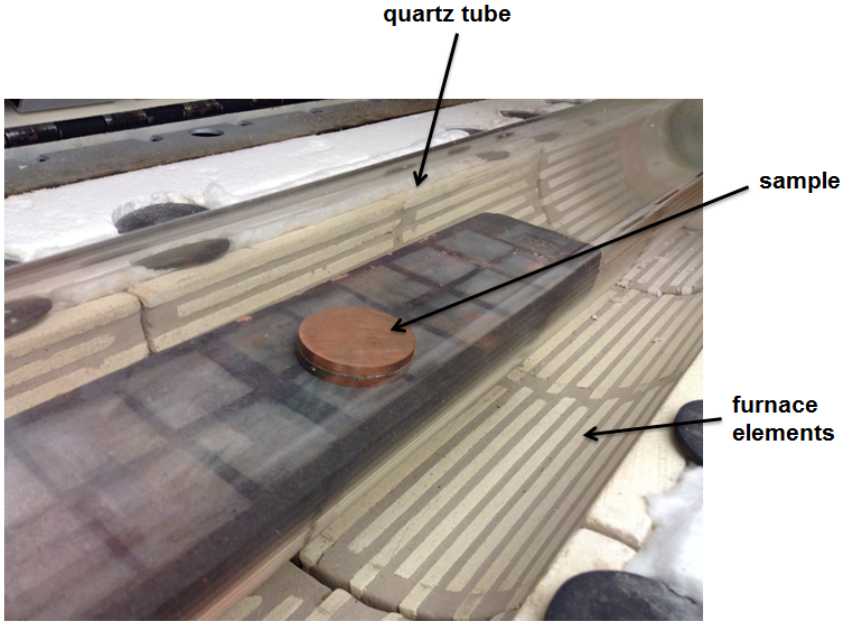

Figure 3.7: Sample Preparation in Thermcraft Tube Furnace

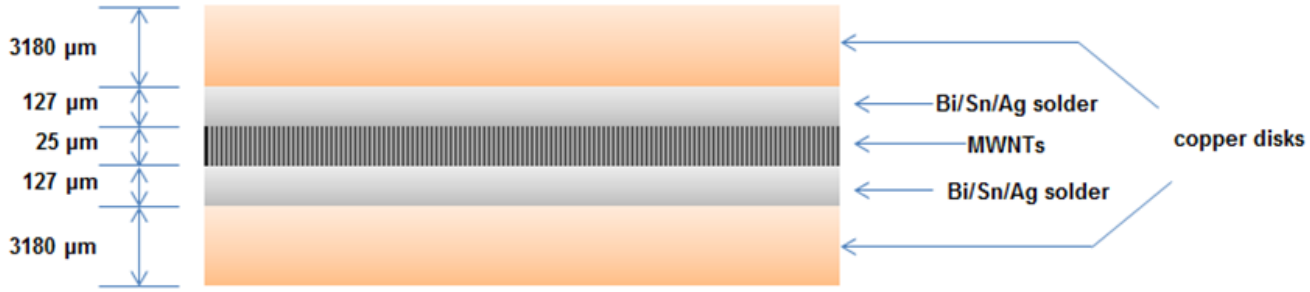

Figure 3.8: Cu-Solder-MWNTs-Solder-Cu Configuration and Approximate Thicknesses

Chapter 4

Testing Approach

Various testing methods exist to determine the performance of a thermal interface material (TIM). The performance of a TIM can be determined by measuring its thermal resistance at an interface, which is found by measuring the temperature difference across the interface per heat flux quantity transported across that interface. Some testing techniques include steady state and transient methods such as transient thermo reflectance measurement, the 3-omega method, and the primary steady-state method called the ASTM D5470. The ASTM D5470 method involves placing the test sample between a hot meter bar and a cold meter bar, through which a certain heat flux is generated [30]. The meter bars consist of multiple temperature sensors, which gauge the temperature drop across the test sample. The total thermal resistance per unit area, which includes the thermal resistance of the TIM and the contact resistance of the TIM-substrate interfaces, is measured as a function of TIM thickness. This testing method is viable under certain assumptions, which are one-dimensional heat flow, constant TIM thickness, and thickness independent contact resistance [30]. In this study, an Analysis Tech ASTM 5470 TIM tester, which can be seen in Figure 4.1, was used. For this apparatus, the heat traveled through the upper meter bar while a chiller cooled the lower meter bar. Thermally-insulating sleeves were accessible to sheath the meter bars in order to reduce heat losses to the surroundings. The TIM tester included an LVDT sensor that measured the in-situ TIM thickness. The testing surfaces of this apparatus were made of highly-smoothed nickel plates with 7-8 μm flatness. The tester also permitted analysis under a range of pressures from 5 to 380 psi and used a pressure sensor with an accuracy of +/- 2.5 psi in the 5 to 95 psi range.

Figure 4.1: Analysis Tech TIM Tester 1400

Since carbon nanotubes (CNTs) are not a traditional thermal interface material (TIM), some modifications were made to the ASTM 5470 TIM tester so that the thermal performance of the CNT array could be established. Alloy 110 copper disks with 33 mm diameters and thicknesses of 3.18 mm were soldered to both sides of the NanoLab CNT array. The copper disks were highly smooth with a 7-8 μm flatness. The TIM configuration to be tested can be placed between the two nickel testing disks of the TIM tester, as shown in Figure 4.2. Xiameter PMX-200 silicone oil was inserted between the nickel/copper interfaces to create better contact between the test surfaces and copper disks. In order to detect the temperature differential across the CNT array TIM, high precision thermistor probes with 1 mm diameters and accuracies of 0.05°C were inserted into 1.2 mm diameter holes that were drilled into the copper disks, as seen in Figure 4.3. Laird Tech TGrease 880 thermal grease was injected into the holes to reduce contact resistances between the probes and the walls of the holes.

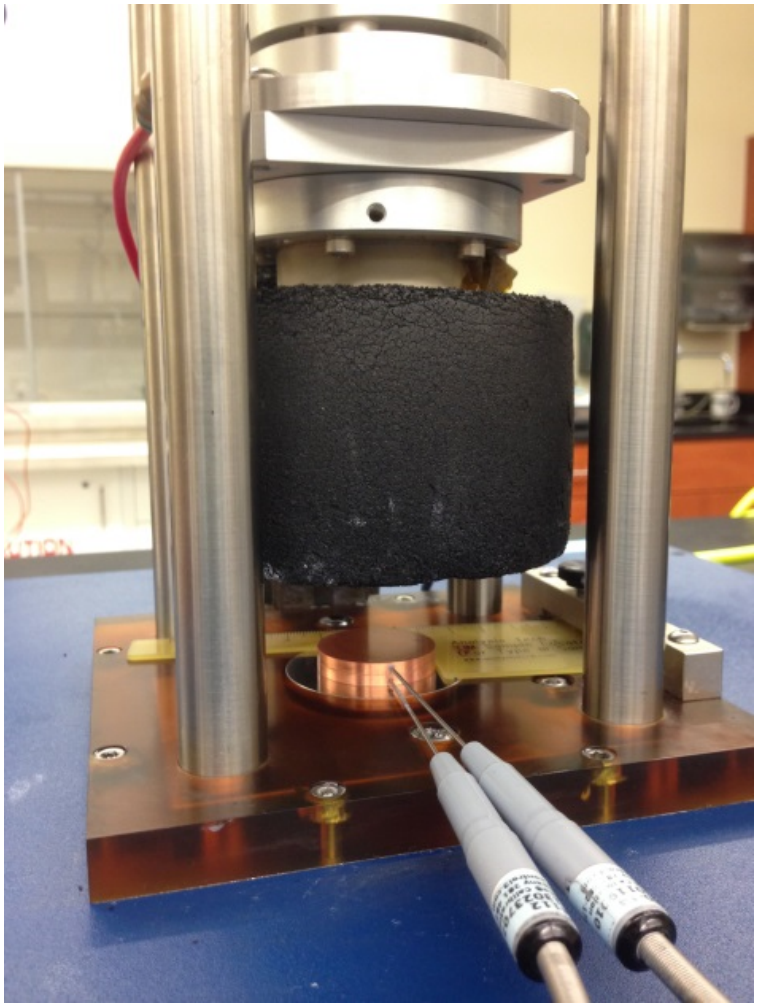

Figure 4.2: Modified TIM Tester Setup

Figure 4.4 displays the Alloy 110 copper disk assembly used to test non-traditional TIMs. The thermal conductivity of the Alloy 110 copper disks was about 388 $\frac{W}{m-K}$. Since the high precision thermistors measured T_1 and T_2, the surface temperatures of the TIM which are labeled T_{s1} and T_{s2}, are calculated according to Equation 4.1 and 4.2. In Equation 4.1 and 4.2, Q" is the heat flux (Q/A) applied to the configuration, l is the distance from the center of the drilled hole to the edge of the copper disk, and K is the thermal conductivity of the copper disks. The temperature difference ΔT across the TIM is calculated with Equation 4.3. It is important to note that the temperature difference is affected by probe disturbance

Figure 4.3: Alloy 110 Copper Disks

since the thermistor probes reside in the heat flow path. Therefore, ΔT is a function of T_1, T_2, Q", l, K, and probe disturbance.

$$T_{s1} = T_1 - \frac{Q''l}{K} \tag{4.1}$$

$$T_{s2} = T_2 - \frac{Q''l}{K} \tag{4.2}$$

$$\Delta T = T_{s1} - T_{s2} = T_1 - T_2 - \frac{2Q''l}{K} \tag{4.3}$$

The root-sum-square method, seen in Equation 4.4, is used to determine the uncertainty with a 95% confidence for measuring ΔT (Carlberg, et al.). With thermal resistance being represented by Equation 4.5, the uncertainty in thermal resistance can be found with Equation 4.6.

$$U\Delta T = \sqrt{(\sum_{i=1}^{n}(\frac{\partial \Delta T}{\partial X_i}\partial X_i))^2} \tag{4.4}$$

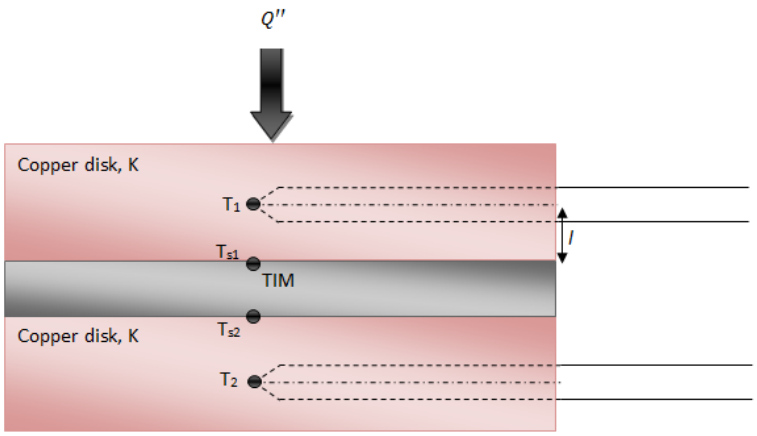

Figure 4.4: Alloy 110 Copper Disks

$$R = \frac{\Delta T}{Q''} \tag{4.5}$$

$$\frac{UR}{R} = \sqrt{(\frac{U\Delta T}{\Delta T})^2 + (\frac{UQ''}{Q''})^2} \tag{4.6}$$

The particular steps taken to test the thermal properties of the copper-CNT disk sample were as follows. The first step was to clean the copper disks by removing any oxidation that formed on the surfaces with a hydrochloric acid-water solution. The disks were then wiped clean with plain water in order to remove any hydrochloric acid residue. Xiameter PMX-200 silicone oil was used to fill the holes inside the copper disks to minimize contact resistances between the thermistor probes and the walls of the drilled holes. A few drops of Xiameter PMX-200 silicone oil were placed on the bottom test surface of the TIM tester to minimize contact resistance between the bottom copper disk surface and lower test surface. The copper-CNT disk sample was placed on the Xiameter silicone oil drops and aligned with the upper test surface of the TIM tester. A few drops of the Xiameter silicone oil was also dropped on the surface of the top copper disk, and the upper testing surface was lowered to meet the surface of the top copper disk. Next, the desired testing pressure was applied. The

thermistor probes were dipped in TGrease 880 thermal grease and inserted into the drilled holes of the copper disks. Any excess of silicone oil or thermal grease was removed before beginning testing. The insulating sleeve was lowered around the sample, and thermal testing at the chosen pressure and temperature was commenced.

Chapter 5

Results and Discussion

As mentioned previously, an Analysis Tech ASTM 5470 TIM tester was used to measure the thermal performance of the sample shown in Figure 3.7. The first set of testing included four continuous tests completed at 20 psi and five continuous tests completed at 50 psi. All tests were conducted at 90°C. Since two 0.0127 cm layers of the Indalloy 282 solder with an approximate thermal conductivity of 0.19 $\frac{W}{cm-K}$ were used to fabricate the sample, the anticipated thermal resistance was about 0.134 $\frac{cm^2-K}{W}$. The first set of 20 psi thermal performance tests resulted in an average thermal resistance of around 0.754 $\frac{cm^2-K}{W}$ with a standard deviation of about 0.002. The individual thermal resistance values obtained from the testing at 20 psi are shown in Figure 5.1. The first set of 50 psi thermal performance tests resulted in an average thermal resistance of about 0.732 $\frac{cm^2-K}{W}$ with a standard deviation of around 0.009. The individual thermal resistance values obtained from testing at 50 psi are shown in Figure 5.2. The higher than expected thermal resistances may have been due to uneven disk surfaces. In other words, the disk surfaces that came in contact with the testing plates were not parallel. Non-parallel surfaces could have resulted in uneven heat flow through the sample. Voids within the solder layer were another possible occurrence that may have affected the attained thermal resistance values.

Since the measured thermal resistance values from the first set of tests were much higher than expected, the test sample was altered via solder reflow under 0.65 psi to realign the copper disks. To achieve this, the sample was heated on a hot plate to the melting temperature of the solder, which was around 140°C. Then, a 500 gram weight was placed on top of the sample. The hot plate was turned off, and the sample was allowed to cool before

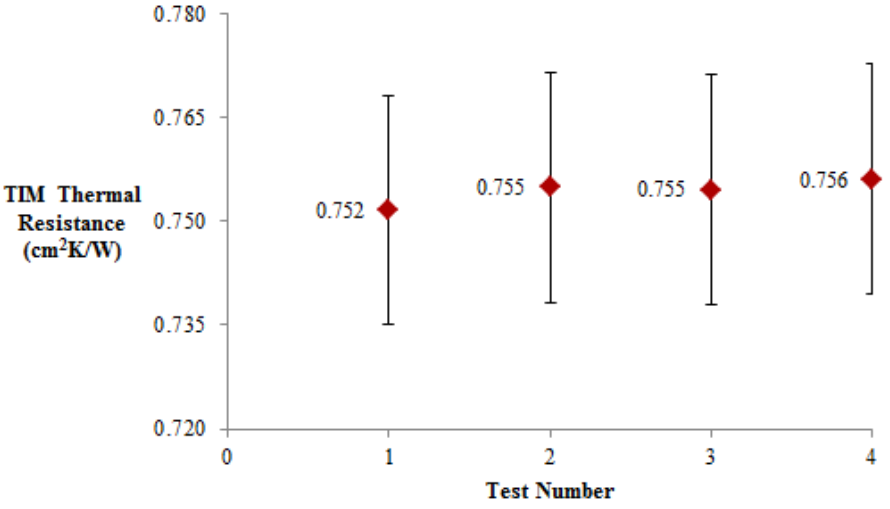

Figure 5.1: Thermal Performance at 20 psi before reflow with an Average Estimated Accuracy within 2.2%

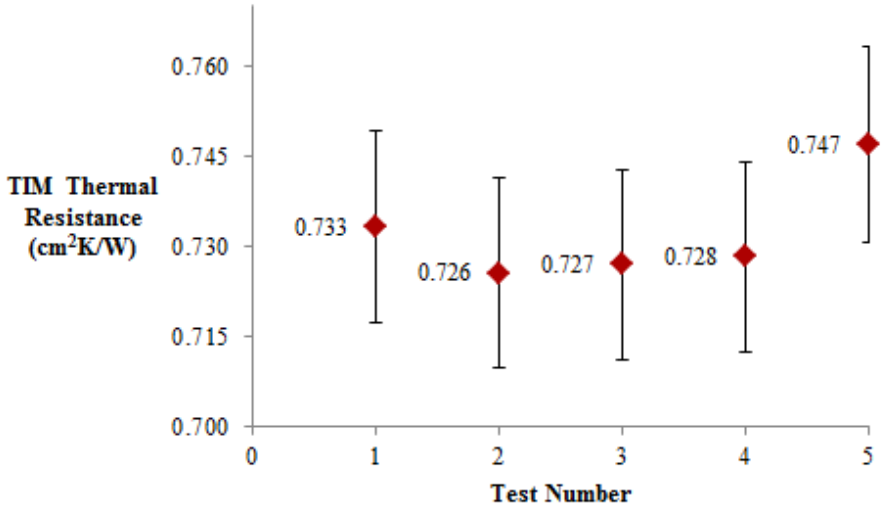

Figure 5.2: Thermal Performance at 50 psi before reflow with an Average Estimated Accuracy within 2.18%

Table 5.1: Thermal Resistance Data at 20 psi after solder reflow

Pressure (psi)	Total Sample Thickness (cm) +/- 0.00254 cm	TIM Thermal Resistance (cm^2K/W)
20	0.647	0.457
20	0.647	0.458
20	0.648	0.461
20	0.647	0.460
20	0.648	0.456
AVERAGES	0.647	0.458

Table 5.2: Thermal Resistance Data at 50 psi after solder reflow

Pressure (psi)	Total Sample Thickness (cm) +/- 0.00254 cm	TIM Thermal Resistance (cm^2K/W)
50	0.649	0.439
50	0.649	0.423
50	0.649	0.440
50	0.649	0.436
50	0.649	0.438
50	0.649	0.435
AVERAGES	0.649	0.435

removing it from the hot plate. This process removed some excess solder from the interface and possibly eliminated any voids in the interface.

A second set of testing using the same pressures and temperature was performed on the modified sample. A 39% decrease in the average thermal resistance was observed at 20 psi with the average thermal resistance being about 0.458 $\frac{cm^2-K}{W}$. At 50 psi, a 41% decrease was observed with the average thermal resistance being around 0.435 $\frac{cm^2-K}{W}$. The individual thermal resistance values obtained at 20 psi and 50 psi after solder reflow of the sample can be viewed in Table 5.1 and 5.2, respectively. Figure 5.3 and Figure 5.4 demonstrate the variation of thermal resistance measurements during testing. The decrease in the thermal resistance values was attributed to the reduced sample thickness after solder reflow. The sample modification may have also eliminated any remaining voids within the interface.

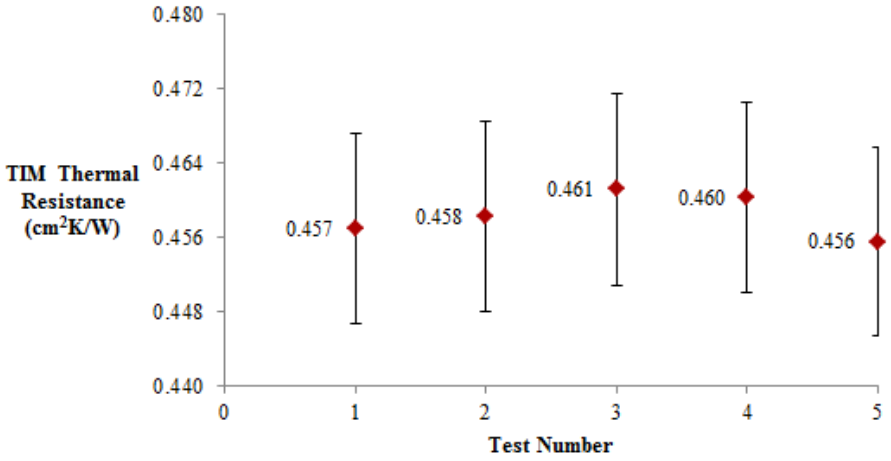

Figure 5.3: Thermal Performance at 20 psi After Solder Reflow with an Average Estimated Accuracy within 2.24%

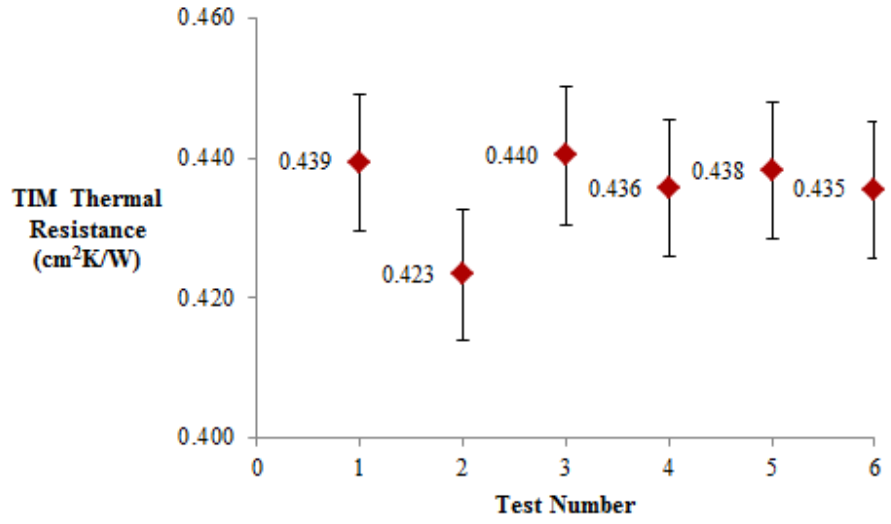

Figure 5.4: Thermal Performance at 50 psi After Solder Reflow with an Average Estimated Accuracy within 2.23%

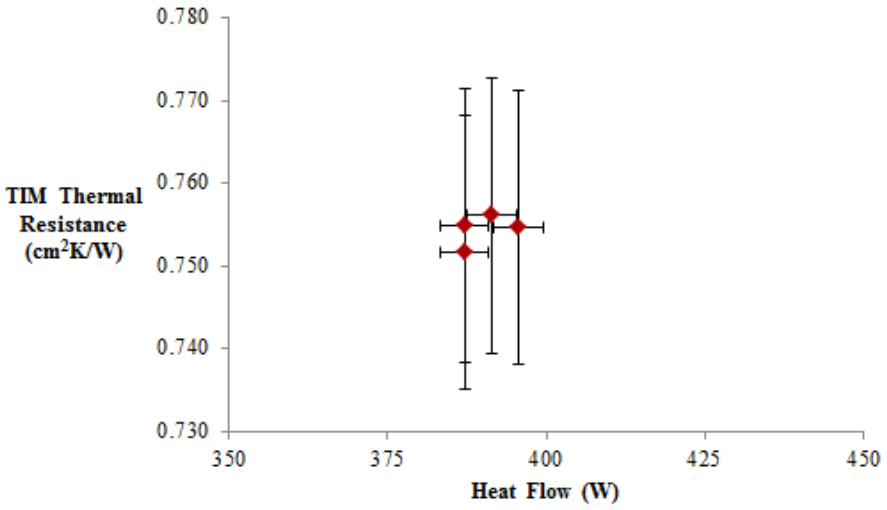

Figure 5.5: Effect of Heat Flow on TIM Thermal Resistance at 20 psi before solder reflow

The effect of the varying heat flow on the thermal resistance before sample modification is shown in Figure 5.5, Figure 5.6, Figure 5.7, and Figure 5.8. The measured heat flow values were accurate within approximately 1%. It can be deduced that the level of heat flow had no noticeable effects on the obtained thermal resistances. Figure 5.9 examines the pressure effects on the total thermal resistance values after realignment of the sample. The pressure measurements were accurate within +/- 2.5 psi for the applied pressures. For the testing at 20 psi, the total thermal resistance values were between 1.50 and 2.00 $\frac{cm^2-K}{W}$. The total thermal resistance value for the 50 psi testing was approximately 1.20 $\frac{cm^2-K}{W}$. Figure 5.10 shows the pressure effects on the TIM thermal resistance values. At 20 psi, the thermal resistance values of the TIM were found in the range of 0.456 to 0.461 $\frac{cm^2-K}{W}$. For 50 psi, the thermal resistance values ranged from approximately 0.423 to 0.440 $\frac{cm^2-K}{W}$. These results suggest that the sample experienced minor pressure dependence most likely due to incomplete contact between the CNTs and the e-beamed gold layer. Therefore, a higher pressure enabled more CNTs to come in contact with the gold layer, which resulted in a slightly lower thermal resistance value [25].

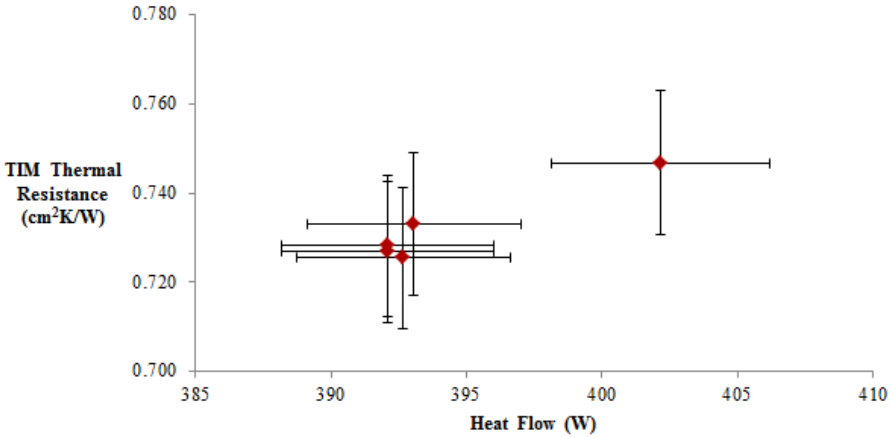

Figure 5.6: Effect of Heat Flow on TIM Thermal Resistance at 50 psi before solder reflow

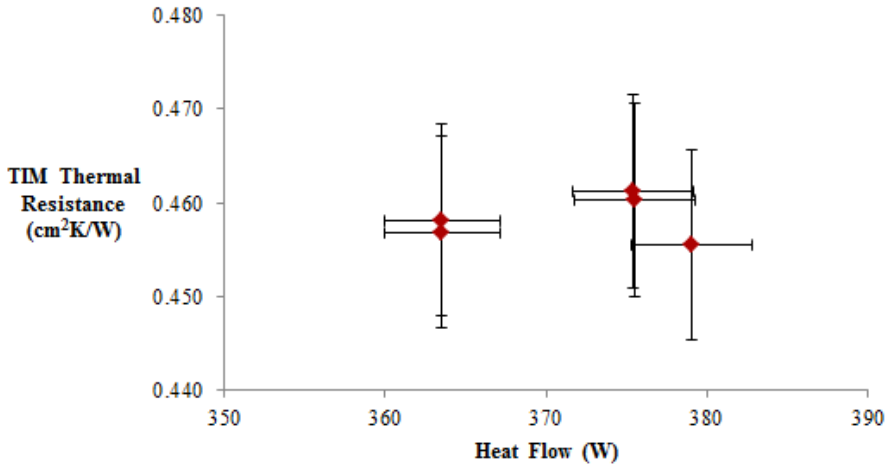

Figure 5.7: Effect of Heat Flow on TIM Thermal Performance at 20 psi after solder reflow

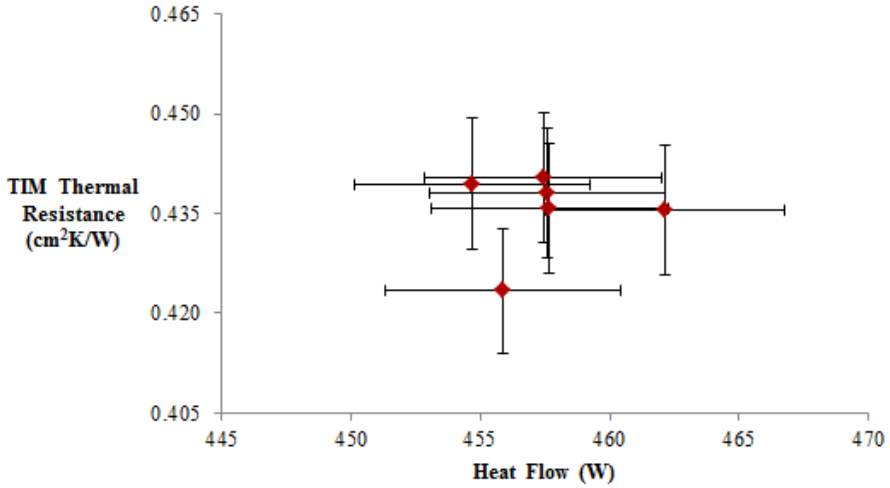

Figure 5.8: Effect of Heat Flow on TIM Thermal Resistance at 50 psi after solder reflow

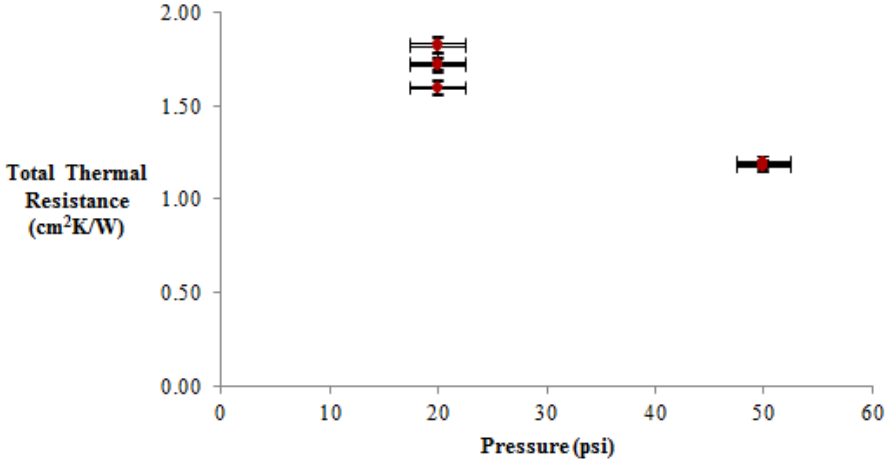

Figure 5.9: Effect of Pressure on Total Thermal Resistance After Solder Reflow

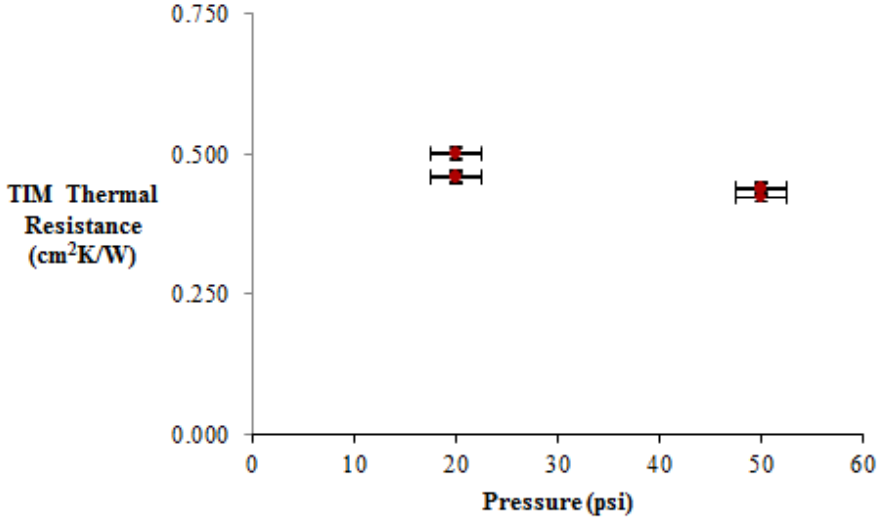

Figure 5.10: Effect of Pressure on TIM Thermal Resistance After Solder Reflow

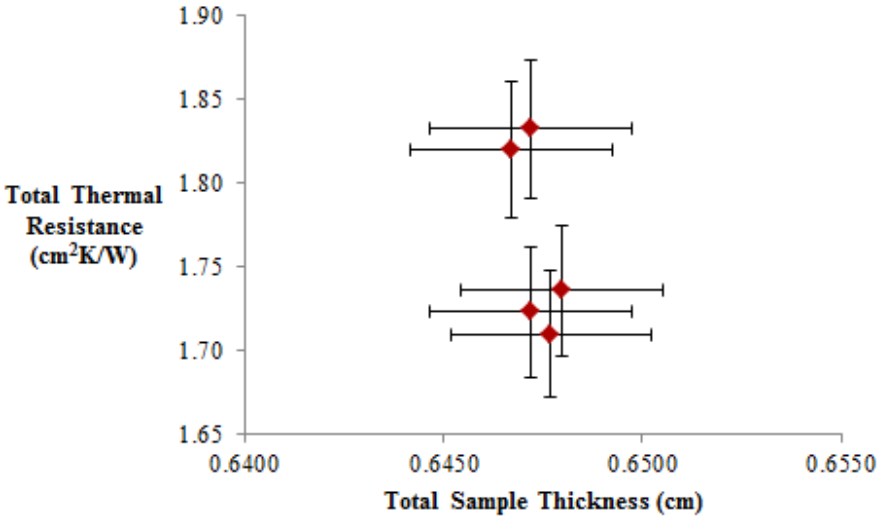

Figure 5.11: Effect of Sample Thickness within +/- 0.00254 cm on Total Thermal Resistance at 20 psi After Solder Reflow with an Average Estimated Accuracy of the Thermal Resistance Value within 2.24%

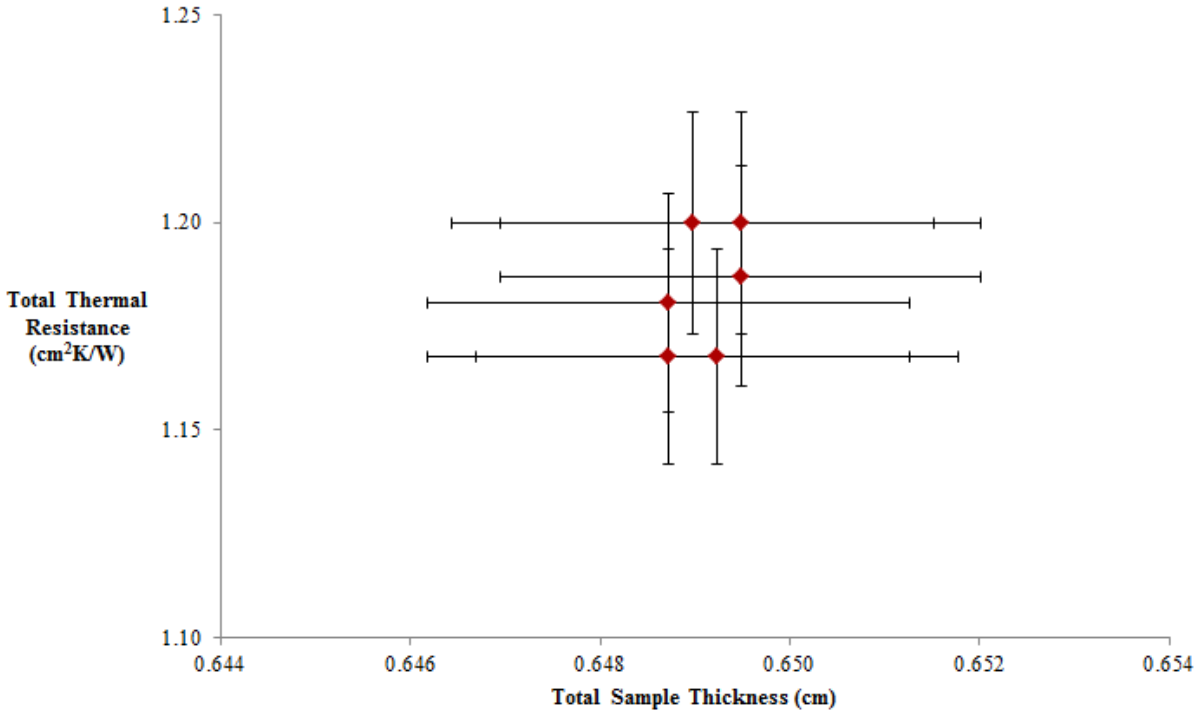

Figure 5.12: Effect of Sample Thickness within +/- 0.00254 cm on Total Thermal Resistance at 50 psi After Solder Reflow with an Average Estimated Accuracy of the Thermal Resistance Value within 2.23%

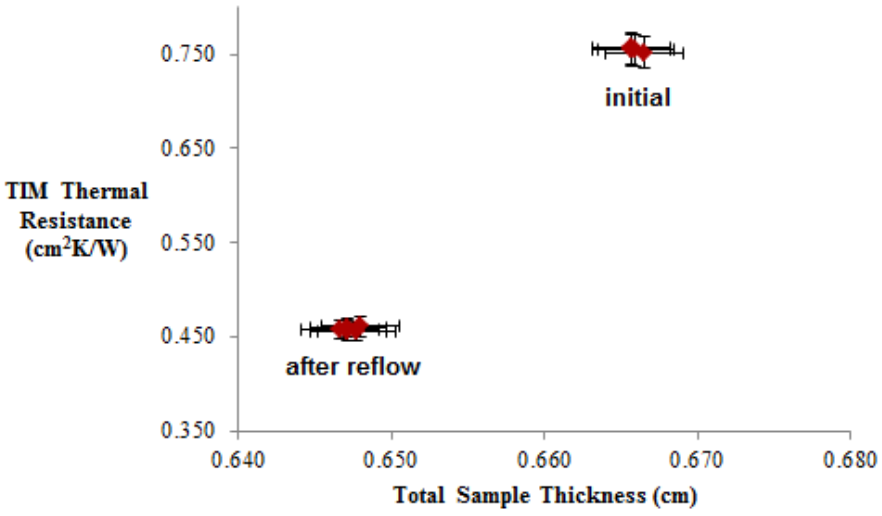

Figure 5.13: Thickness Effects on TIM Thermal Resistance at 20 psi Before and After Solder Reflow with an Estimated Average Accuracy within 2.25%

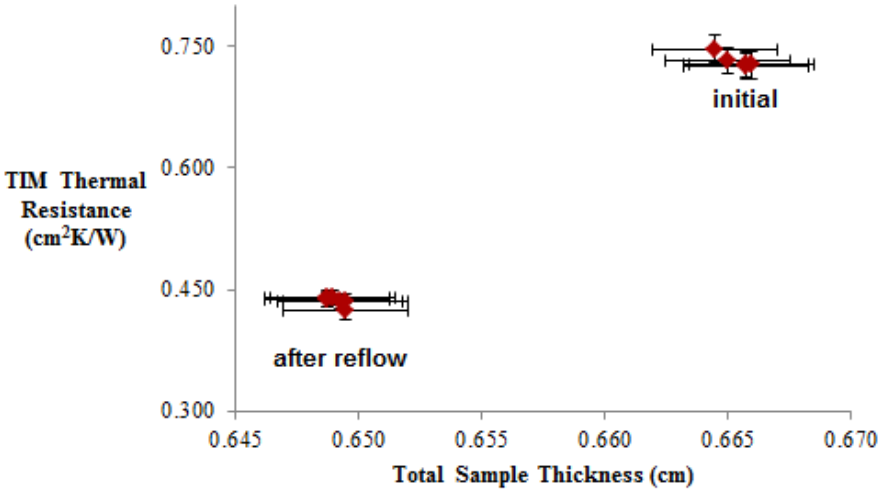

Figure 5.14: Thickness Effects on TIM Thermal Resistance at 50 psi Before and After Solder Reflow with an Estimated Average Accuracy within 2.21%

Figure 5.11 and Figure 5.12 investigate the effects of sample thickness on the total thermal resistance values after modification. For the total sample thickness, the only parameter likely to change was the thickness of the contact greases between the copper surfaces of the sample and the testing surfaces of the TIM tester. No noticeable trends were observed between total sample thickness and the total thermal resistance. Therefore, thickness effects of the overall test sample can be neglected. However, this conclusion does not extend to the TIM joint.

Figure 5.13 and Figure 5.14 observe the difference in the TIM thermal resistance as a function of the total sample thickness. Before the sample realignment, the average thickness of the sample along with the incorporated thermal grease layers used between the copper disks and testing surfaces was approximately 0.665 cm (0.262 inches). After the sample realignment, the average sample thickness was about 0.648 cm (0.255 inches), meaning the total sample thickness was reduced by approximately 0.018 cm (0.007 inches). It is important to note that arctic silver thermal grease was required in the first set of testing at the contact interfaces because a thicker contact agent was needed to fill the space between the uneven surfaces, while Xiameter silicone oil was used in the second set of testing. Since arctic silver

is thicker than silicone oil, part of the decrease in the total sample thickness was due to the different contact agents used. Figure 5.13 shows that the TIM thermal resistance values were around 0.751 $\frac{cm^2-K}{W}$ for a total sample thickness around 0.665 cm (0.262 inches) before modification of the sample and 0.451 $\frac{cm^2-K}{W}$ for a total sample thickness around 0.648 cm (0.255 inches) after sample modification at 20 psi testing. Similarly for 50 psi, Figure 5.14 displays TIM thermal resistance values slightly lower than 0.750 $\frac{cm^2-K}{W}$ for a total sample thickness around 0.665 cm (0.262 inches) before modification of the sample, and it shows thermal resistance values slightly lower than 0.450 $\frac{cm^2-K}{W}$ for a total sample thickness around 0.648 cm (0.255 inches) after the sample realignment.

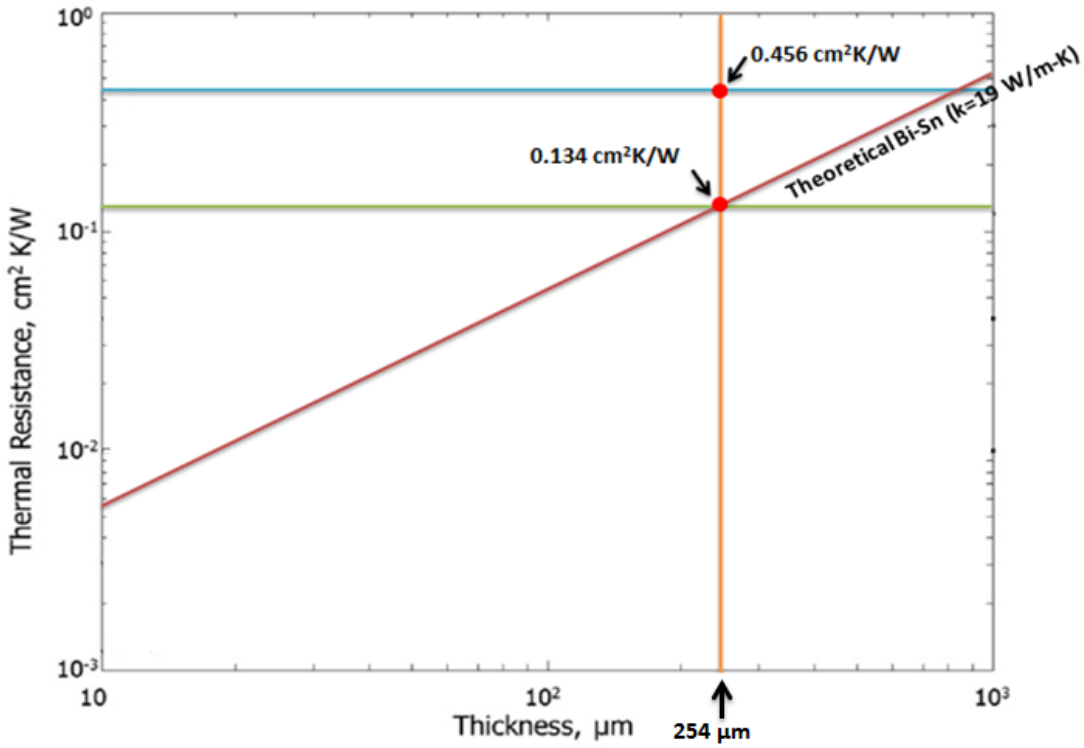

Figure 5.15: Theoretical and Experimental Thermal Resistances of Various TIMs as a Function of Thickness

Figure 5.15 presents theoretical and experimental thermal resistances for several solder TIMs as a function of the solder thickness in microns. The theoretical thermal resistance values for a Bi-Sn solder with a thermal conductivity of approximately 19 $\frac{W}{m-K}$ is shown by

the maroon line. For a solder thickness of about 0.0254 cm, or 254 microns, the theoretical thermal resistance was calculated to be about 0.134 $\frac{cm^2-K}{W}$, which is shown by the red dot that resides at the intersection between the orange and green line in Figure 5.15. The lowest experimental thermal resistance value that was achieved was about 0.456 $\frac{cm^2-K}{W}$ and is demonstrated by the red dot at the intersection of the orange and blue line. In previous research, a similar thermal resistance value of 0.430 $\frac{cm^2-K}{W}$ was achieved for an open-ended CNT assembly consisting of carbon nanotubes bonded to a copper substrate with a tin-lead solder. The CNT film height in the CNT assembly was approximately 180 μm [23].

In this study, a CNT-solder TIM using vertically-aligned CNTs (VACNTs) and a bismuth/tin/silver solder was fabricated. The CNT-solder TIM was bonded between two copper disks for testing purposes. The thermal performance of the copper disk-solder-CNT-solder-copper disk configuration was tested using an ASTM 5470 Thermal Interface Material Analyzer and highly accurate thermistor probes, which measured the temperature drop across the CNT-solder interface. Thermal performance testing was completed at pressures of 20 psi and 50 psi. While the expected thermal resistance value of the TIM interface was 0.134 $\frac{cm^2-K}{W}$, the assessed TIM thermal resistance values were about 0.726 to 0.756 $\frac{cm^2-K}{W}$ before alteration of the sample through solder reflow and 0.423 to 0.461 $\frac{cm^2-K}{W}$ after solder reflow. Slight pressure dependence was seen for testing at 20 psi versus 50 psi, which was possibly due to better contact between the testing surfaces and sample.

Chapter 6

Conclusions and Final Recommendations

From the formerly discussed research and experiments, it can be concluded that vertically-aligned CNTs (VACNTs) are practical for use as thermal interface materials (TIMs). CNTs possess multiple qualities that make them ideal for TIM applications such as high thermal conductivities, good conformability, considerable mechanical strength, and substantial resiliency. Many factors influence the thermal performance of CNT array (CNA) TIMs. These factors include, but are not limited to, CNA density, CNA height, nanotube diameter, CNT alignment, and CNT quality. Other issues that affect thermal performance of CNA TIMs are the interfacial thermal resistances between the CNT free ends and opposing substrates as well as the interfacial thermal resistances between the CNA and its growth substrate. It was also reported that multi-walled CNTs (MWNTs) are superior to single-walled CNTs (SWNTs) for thermal transport applications since MWNTs possess more paths for heat transfer. Additionally, the solid solder CNT composite can potentially improve joint resiliency with coefficient of thermal expansion (CTE) mismatches involving solder joints in electronics packaging.

Other obstacles related to generating CNA TIMs involve large-scale manufacturing issues and growth substrate removal. Like other products, CNTs are less expensive when produced in bulk. However, high volume production of CNTs requires larger furnaces for chemical vapor deposition (CVD) fabrication, and larger furnaces result in less control over the quality and parameters of CNTs [27]. The competition for this type of product, a solder-CNA composite TIM, is currently very small. Some others are exploring similar technologies, but solder-CNA composite TIMs are not commercially available presently. This type of technology can only be created by those with specialized expertise related to this

field. One potential risk of this product is the demand not being high enough to outweigh the cost the of the product. As previously discussed, removing the silicon growth substrate in this research required using a hydrofluoric (HF) acid bath that was diluted with deionized water. This process has potential health risks if not carried out properly since HF acid is a very potent acid. Completing a substrate detachment process on a large-scale basis may be cumbersome and time-consuming if the process is not optimized. However, another potential method reported by Cross et al. [25] to weaken the bond between the CNTs and their growth substrate was by introducing a water vapor into the CVD fabrication chamber after nanotube growth.

Since NanoLab Inc. only completes certain sample analyses on a case-by-case basis, performing transmission electron microscopy (TEM) on the CNA samples is necessary to determine certain CNT parameters such as individual CNT diameter and bundle diameter [31]. According to Baitinger et al. [32], TEM is also an effective technique to ascertain the local density of MWNTs. Another evaluation to be considered is atomic force microscopy (AFM), which is useful tool in detecting nanotube lengths [31]. Knowing the approximate nanotube diameter as well as the density of the CNA would enable one to determine the CNT area coverage percentage, as calculated by Equations 2.3 through 2.6.

In order to determine the effect of CNAs on solder joint life, it is recommended that a stress/strain analysis be completed under thermal cycling conditions. Thermal aging tests are also suggested so that the thermal performance of the CNA-solder composite TIM can be examined. Various types of solder should also be explored to determine whether any wetting effects exist between the CNTs and solder. Examining the effects of different solder types in this type of configuration would also be beneficial in order to determine the most effective solders to use for specific systems or applications.

Table 6.1 shows the thermal resistance values obtained for some CNA configurations similar to the constructed CNT-solder composite TIM in the current study. The first configuration shown in Table 6.1 consisted of a CNA with a height of 30 microns and demonstrated

Table 6.1: Comparison of Thermal Performance of Similar CNA Configurations

Sample Configuration	CNA Height (µm)	Foil/Solder thickness (µm)	Foil/Solder Thermal Conductivity (W/m/K)	Thermal Resistance (cm^2-K/W)	Error	Reference
Si-Ti/Fe-CNA-Ti/Au-Ag foil	30	25	≈ 429	0.100	±0.005	from Cross et al.
Si-Ti/Au-CNA-Ti/Au-Ag foil	130	25	≈ 429	0.100	±0.005	from Cross et al.
CNA-solder-Cu	180	-	-	0.430	-	from Zhu et al.
Bi/Sn/Ag solder-Ti/Ni/Au-CNA-Ti/Ni/Au-Bi/Sn/Ag solder	25	254	19	0.456	±2.2%	Current study

a total thermal contact resistance of approximately 0.100 $\frac{cm^2-K}{W}$. The thermal resistance is lower than the obtained thermal resistance in the current study; however, this configuration used a Ti/Fe catalyst layer to grow the CNA. Consequently, there existed a much better bond between the CNTs and the Ti/Fe layer than there would between a CNA and an electron-beamed metal layer. The second sample configuration showed similar results, which suggested that the thermal resistance value was dominated by the interfacial thermal resistances. While both of the CNA sample configurations shown from Cross et al. [25]. exhibited lower thermal resistance values than the CNT-solder composite TIM in the current study, it is important to note that the thickness of the solder layer used in the current study was probably much greater than the Ti/Au and Ti/Fe layers that existed in the sample configuration fabricated by Cross et al. [25]. The total thermal resistance of the one-sided CNA assembly from Zhu et al. [23] was reported to be about 0.430 $\frac{cm^2-K}{W}$. The thickness and type of solder used in this research was not cited, but the CNA height was indicated to be 180 microns. The thickness and thermal conductivity value of the solder are essential in order to better compare the thermal resistance results attained by Zhu et al. [23] to the CNT-solder composite TIM in the current study. Nevertheless, the current study achieved comparable thermal resistance values with a CNA-solder composite TIM that contained two solder layers as opposed to one in the analysis conducted by Zhu et al. [23].

The current research sought to demonstrate feasibility of CNT-solder joint composite TIMs by utilizing high quality MWNTs obtained from NanoLab Inc. The obtained MWNTs

were good quality, vertically-aligned CNT arrays in order to avoid tube-tube resistances. To overcome the interfacial thermal resistance issues, the CNA free ends were soldered to copper disks on both sides through the utilization of "CNT transfer technology." Not only does this type of configuration resolve the thermal resistance issues of the CNT free ends, but it also overcomes the high temperature synthesis problems involved with growing CNAs for TIM applications. This technique promotes efficient CNA fabrication by synthesizing nanotubes on substrates that are known to be successful for high quality CNT growth, and it allows the CNA to be transferred to a chosen substrate which is most compatible and effective for a particular application. The insertion of a CNA in between a solder joint could potentially prolong the solder joint life by strengthening the joint, while continuing to promote heat transfer through the interface. While some research has explored the mechanical effects of adding CNTs in a powdered form to solder [33], it is important to note that there are currently no other known reports of the thermal or mechanical performance of this type of CNT-solder-Cu interface configuration, which uses VACNTs.

References

[1] J Hone. Carbon nanotubes: thermal properties. *Dekker Encyclopedia of Nanoscience and Nanotechnology, Marcel Dekker, Inc., New York*, pages 603–610, 2004.

[2] Baratunde A Cola, Xianfan Xu, and Timothy S Fisher. Increased real contact in thermal interfaces: A carbon nanotube/foil material. *Applied physics letters*, 90(9):093513, 2007.

[3] X Hu, E Pop, H Dai, KE Goodson, MA Panzer, G Zhang, and D Mann. Thermal properties of metal-coated vertically aligned single-wall nanotube arrays. *Journal of Heat Transfer*, 130(5):052401, 2008.

[4] Frank P Incropera, Adrienne S Lavine, and David P DeWitt. *Fundamentals of heat and mass transfer*. John Wiley & Sons, 2011.

[5] Tao Tong, Yang Zhao, Lance Delzeit, Ali Kashani, M Meyyappan, and Arun Majumdar. Dense vertically aligned multiwalled carbon nanotube arrays as thermal interface materials. *Components and Packaging Technologies, IEEE Transactions on*, 30(1):92–100, 2007.

[6] The history of carbon nanotubes - who invented the nanotube?, June 2009. URL `http://nanogloss.com/nanotubes/the-history-of-carbon-nanotubes-who-invented-the-nanotube/#axzz2ZcJsFMv0`.

[7] Carbon nanotubes. eZ Publish, 2009. URL `http://www.nanocyl.com/CNT-Expertise-Centre/Carbon-Nanotubes`.

[8] J Hone, MC Llaguno, NM Nemes, AT Johnson, JE Fischer, DA Walters, MJ Casavant, J Schmidt, and RE Smalley. Electrical and thermal transport properties of magnetically aligned single wall carbon nanotube films. *Applied Physics Letters*, 77(5):666–668, 2000.

[9] Boris I Yakobson and Phaedon Avouris. Mechanical properties of carbon nanotubes. In *Carbon nanotubes*, pages 287–327. Springer, 2001.

[10] Carbon nanotubes. eZpublish, July 2014. URL `http://www.nanocyl.com/en/CNT-Expertise-Centre/Carbon-Nanotubes`.

[11] Jia Choi and Yong Zhang. Properties and applications of single-, double- and multi-walled carbon nanotubes, July 2014. URL `http://www.sigmaaldrich.com/technical-documents/articles/materials-science/single-double-multi-walled-carbon-nanotubes.html`.

[12] Carbon nanotubes and the electrical, thermal, mechanical and other useful properties of carbon nanotubes by cheap tubes, June 2013. URL `http://www.azonano.com/article.aspx?ArticleID=1564`.

[13] Charles A Harper and Ronald N Sampson. *Electronic materials and processes handbook*, volume 3. McGraw-Hill, 2004.

[14] Merrill L Minges. *Electronic materials handbook: packaging*, volume 1. Asm International, 1989.

[15] William D Callister Jr. *Fundamentals of materials science and engineering*. John Wiley & Sons, 2001.

[16] Ali E Aliev, Marcio H Lima, Edward M Silverman, and Ray H Baughman. Thermal conductivity of multi-walled carbon nanotube sheets: radiation losses and quenching of phonon modes. *Nanotechnology*, 21(3):035709, 2010.

[17] Qing Zhang, George Chen, SF Yoon, J Ahn, SG Wang, Q Zhou, Q Wang, JQ Li, et al. Thermal conductivity of multiwalled carbon nanotubes. *Physical Review B*, 66(16): 165440, 2002.

[18] Baratunde A Cola. Carbon nanotubes as high performance thermal interface materials. *ITEMŹ*, page 10, 2010.

[19] Anand Desai, James Geer, and Bahgat Sammakia. A statistical analysis of thermal interface materials enhanced by vertically aligned carbon nanotubes. In *Thermal and Thermomechanical Phenomena in Electronics Systems, 2006. ITHERM'06. The Tenth Intersociety Conference on*, pages 1412–1416. IEEE, 2006.

[20] Jun Xu and Timothy S Fisher. Enhanced thermal contact conductance using carbon nanotube array interfaces. *Components and Packaging Technologies, IEEE Transactions on*, 29(2):261–267, 2006.

[21] Jun Xu and Timothy S Fisher. Enhancement of thermal interface materials with carbon nanotube arrays. *International Journal of Heat and Mass Transfer*, 49(9):1658–1666, 2006.

[22] Y Wu, CH Liu, H Huang, and SS Fan. Effects of surface metal layer on the thermal contact resistance of carbon nanotube arrays. *Applied physics letters*, 87(21):213108–213108, 2005.

[23] Lingbo Zhu, Dennis W Hess, and CP Wong. Assembling carbon nanotube films as thermal interface materials. In *Electronic Components and Technology Conference, 2007. ECTC'07. Proceedings. 57th*, pages 2006–2010. IEEE, 2007.

[24] Michael T Barako, Yuan Gao, Amy M Marconnet, Mehdi Asheghi, and Kenneth E Goodson. Solder-bonded carbon nanotube thermal interface materials. In *Thermal and Thermomechanical Phenomena in Electronic Systems (ITherm), 2012 13th IEEE Intersociety Conference on*, pages 1225–1233. IEEE, 2012.

[25] Robert Cross, Baratunde A Cola, Timothy Fisher, Xianfan Xu, Ken Gall, and Samuel Graham. A metallization and bonding approach for high performance carbon nanotube thermal interface materials. *Nanotechnology*, 21(44):445705, 2010.

[26] Haixia Shang, Jianxin Gao, P Ian Nicholson, and Steve Kenny. An investigation of reliability of solder joints in microelectronic packages by high temperature moiré method. *Microelectronics Reliability*, 51(5):994–1002, 2011.

[27] Mukul Kumar and Yoshinori Ando. Chemical vapor deposition of carbon nanotubes: a review on growth mechanism and mass production. *Journal of nanoscience and nanotechnology*, 10(6):3739–3758, 2010.

[28] Roberta A DiLeo, Brian J Landi, and Ryne P Raffaelle. Purity assessment of multiwalled carbon nanotubes by raman spectroscopy. *Journal of Applied Physics*, 101(6):064307, 2007.

[29] Yang Chai, Jingfeng Gong, Kai Zhang, Philip CH Chan, and Matthrew MF Yuen. Low temperature transfer of aligned carbon nanotube films using liftoff technique. In *Electronic Components and Technology Conference, 2007. ECTC'07. Proceedings. 57th*, pages 429–434. IEEE, 2007.

[30] Márta Rencz. Testing interface thermal resistance. In *Electronics Packaging Technology Conference, 2007. EPTC 2007. 9th*, pages 272–277. IEEE, 2007.

[31] K Safarova, R Kubinek, M Vujtek, and A Rek. Usage of afm, sem and tem for the research of carbon nanotubes. 2007.

[32] EM Baitinger, NA Vekesser, IN Kovalev, OV Slobodchikov, and VV Viktorov. Transmission electron microscopic study of multiwalled carbon nanotubes. *Inorganic Materials*, 47(6):614–617, 2011.

[33] YD Han, HY Jing, SML Nai, LY Xu, Cher Ming Tan, and J Wei. Interfacial reaction and shear strength of ni-coated carbon nanotubes reinforced sn–ag–cu solder joints during thermal cycling. *Intermetallics*, 31:72–78, 2012.

Appendices

Appendix A

Theoretical Thermal Resistance Value of the Solder Interface

Since the total thickness of the solder was 0.0254 cm,

$$0.01\,in = 0.0254\,cm \tag{A.1}$$

and the approximate thermal conductivity of the solder was 0.19 $\frac{W}{cm-K}$, the theoretical thermal resistance was about 0.134 $\frac{cm^2-K}{W}$.

$$R_{th} = \frac{l}{K} = \frac{0.0254\,cm}{0.19\,\frac{W}{cm-K}} = 0.134\,\frac{cm^2-K}{W} \tag{A.2}$$

where R_{th} is the thermal resistance, l is the thickness of the solder layer, and K is the thermal conductivity of the solder.